Stochastic Resilience Thresholds and Early Warning Signals in Water-Energy-Food Systems: A Safety Science Framework for Preventing Catastrophic Transitions

Mohammad Fazle Rabbi

PII: S2666-4496(26)00026-5
DOI: https://doi.org/10.1016/j.jnlssr.2026.100304
Reference: JNLSSR 100304

To appear in: *Journal of Safety Science and Resilience*

Received date: 26 October 2025
Revised date: 26 December 2025
Accepted date: 3 February 2026

Please cite this article as: Mohammad Fazle Rabbi , Stochastic Resilience Thresholds and Early Warning Signals in Water-Energy-Food Systems: A Safety Science Framework for Preventing Catastrophic Transitions, *Journal of Safety Science and Resilience* (2026), doi: https://doi.org/10.1016/j.jnlssr.2026.100304

Highlights

- Stochastic resilience framework detects 82 catastrophic transitions with 20-78 time steps advance warning
- Cross-sectoral cascade amplification quantified: 70% water shock propagates to 14% energy and 10% food failures
- Variance-autocorrelation algorithms outperform deterministic thresholds in detecting noise-induced infrastructure collapse
- Framework validated across energy grids, flood systems, earthquake cascades, and pandemic healthcare surge scenarios
- Adaptive governance module enables real-time emergency coordination during multi-sectoral infrastructure failures

Stochastic Resilience Thresholds and Early Warning Signals in Water-Energy-Food Systems: A Safety Science Framework for Preventing Catastrophic Transitions

Mohammad Fazle Rabbi[a],*

[a],* Coordination and Research Centre for Social Sciences, Faculty of Economics and Business, University of Debrecen, Böszörményi út 138, 4032 Debrecen, Hungary.

* Corresponding Author: drrabbikhan@gmail.com; or rabbi.mohammad@econ.unideb.hu

Abstract: Water-energy-food infrastructure systems face catastrophic transition risks as climate change intensifies cross-sectoral interdependencies. Prevailing safety methodologies exhibit critical limitations: deterministic frameworks overlooking stochastic resilience thresholds, inadequate early warning capabilities lacking operational protocols, and sectoral isolation underestimating cascade propagation. This study introduces the Stochastic Resilience and Early Warning Framework (SREWF), synthesizing resilience theory, panarchy, and stochastic viability theory into operational modules for catastrophic transition prevention. The framework integrates stochastic resilience thresholds, variance and autocorrelation-based detection algorithms, equity-adjusted safety boundaries, and cascade prevention mechanisms capturing noise-induced collapse and cross-sectoral feedback amplification. Validation across 100 parameter scenarios achieves perfect classification under controlled simulation conditions (82/82 collapses detected, 18/18 stable trajectories), though operational field deployment expects 80-90% accuracy accounting for measurement errors and unmodeled disturbances, consistent with empirical early warning systems. Average lead times reach 39.3 time steps (representing approximately 8-10 months advance warning, with minimum 20 time steps under worst-case conditions). Cross-sectoral cascade analysis reveals 70% water shocks trigger 14.1% energy and 10.3% food secondary impacts, validating coupling coefficients against documented failures. Parameter sensitivity testing demonstrates operational robustness, with 80% of tested combinations maintaining safe-zone operation. Beyond water-energy-food systems, the framework demonstrates transferability to flood early warning, earthquake cascades, energy grid stability, and healthcare surge management. These findings advance catastrophic transition prevention methodology aligned with Sendai Framework principles, providing emergency managers validated tools for protecting vulnerable populations during cascading infrastructure failures.

Keywords: Early warning systems; Cascading failures; Critical infrastructure resilience; Stochastic resilience thresholds; Disaster risk reduction; Water-energy-food systems

***Complete nomenclature and abbreviations are provided in Appendix A.**

1. Introduction

Safety-critical infrastructure systems face unprecedented challenges as climate change, resource scarcity, and socioeconomic pressures intensify cross-sectoral interdependencies within water-energy-food systems [1,2]. The 2023 UN Water Development Report documents that 2.3 billion people face water scarcity affecting food production and energy generation across 80 countries, with climate induced infrastructure failures causing annual economic losses exceeding USD 200 billion globally [3]. The UNECE nexus assessment identifies cross sectoral interdependencies as amplifying disaster risks by 40 to 60 percent

compared to isolated sectoral failures, particularly in water energy food systems where cascading disruptions disproportionately affect vulnerable populations [4]. The Millennium Drought (1997–2009) in Australia's Murray-Darling Basin exemplifies catastrophic transition dynamics, where water scarcity triggered cascade failures across irrigation networks, hydropower generation, and agricultural production, resulting in estimated economic losses exceeding AUD $5.7 billion and permanent ecosystem degradation [5]. Conventional risk assessment frameworks failed to detect these impending threshold crossings despite observable precursor signals including declining reservoir storage rates showing increasing temporal autocorrelation three months before collapse, rising variance in agricultural water allocations indicating system instability, and cross sectoral coupling amplification where energy sector stress began affecting irrigation reliability two seasons before widespread crop failures [6,7]. These failures highlight fundamental inadequacies in current safety science methodologies treating infrastructure failures as independent events rather than interconnected cascade dynamics characteristic of complex adaptive systems [8].

While catastrophic transition risks affect diverse critical infrastructure domains, this study focuses specifically on water-energy-food (WEF) systems for three methodological and empirical reasons. First, WEF systems exhibit uniquely strong bidirectional interdependencies where each sector simultaneously serves as input and constraint for the others, creating tightly coupled feedback networks where cascade propagation is particularly rapid and severe [9,10]. Second, climate change disproportionately affects WEF systems through direct environmental pathways (precipitation variability, temperature extremes), making these systems priority targets for stochastic resilience analysis under deepening environmental uncertainty [11]. Third, WEF infrastructure failures directly threaten human survival through disruptions to essential life support services (potable water, food security, heating and cooling), distinguishing these systems from other critical infrastructure where failures primarily affect economic productivity rather than immediate mortality risks [3,12].

Recent infrastructure collapse events reveal systematic patterns absent from conventional safety assessment approaches. The 2021 Texas power crisis demonstrated cross-sectoral cascade propagation where natural gas supply failures triggered electricity grid collapse, subsequently disrupting water treatment facilities serving 12 million residents [13]. South Africa's ongoing water-energy crisis illustrates persistent vulnerabilities where electricity shortages compromise water pumping infrastructure, creating feedback loops that amplify both sectoral failures [14]. These catastrophic transitions share critical characteristics: gradual stress accumulation followed by abrupt system-wide collapse, cross-sectoral cascade propagation through interdependency networks, and delayed emergency response due to inadequate early warning detection capabilities [15].

Current safety science approaches exhibit three critical limitations impeding effective catastrophic transition prevention in water-energy-food infrastructure systems [16,17]. First, deterministic risk assessment frameworks fundamentally mischaracterize stochastic threshold dynamics where random fluctuations can trigger regime shifts when systems approach critical bifurcation points [18,19]. Conventional approaches assume predictable, noise-free dynamics despite empirical evidence demonstrating that environmental variability and governance uncertainties introduce stochastic perturbations capable of precipitating collapse even when deterministic models predict stability [20]. This deterministic bias prevents emergency managers from quantifying probabilistic threshold crossing risks essential for proactive intervention planning under uncertainty.

Second, existing frameworks lack operational early warning detection algorithms capable of identifying precursors to catastrophic transitions with sufficient advance notice for preventive intervention deployment.

While critical slowing down theory demonstrates that systems approaching bifurcation points exhibit increasing variance and temporal autocorrelation, translation of these theoretical indicators into validated operational protocols remains underdeveloped [21,22]. Emergency managers require quantitative benchmarks specifying detection accuracy, lead times, false positive rates, and intervention windows across diverse parameter scenarios representative of real-world uncertainty conditions.

Third, safety assessment methodologies treat sectoral failures as independent events, do not capture cross-sectoral cascade propagation mechanisms through which localized disturbances trigger system-wide collapse [23]. Water-energy-food systems exhibit strong interdependencies where supply disruptions in one sector propagate through coupling networks affecting multiple interconnected domains [24]. Conventional single-sector risk assessment approaches systematically underestimate cascade risks by neglecting interdependency dynamics, resulting in emergency response protocols inadequately calibrated for compound failure scenarios.

Three research questions guide this investigation, directly addressing these methodological gaps. First, how can stochastic resilience thresholds be operationally quantified to capture noise-induced collapse dynamics, providing probabilistic risk assessment capabilities absent from deterministic frameworks? Second, what early warning indicators reliably precede catastrophic transitions with sufficient lead times for preventive intervention, and how do detection accuracy, false positive rates, and intervention windows perform across diverse parameter scenarios representative of real-world uncertainty? Third, how do cross-sectoral cascades propagate through water–energy–food interdependency networks, what coupling mechanisms govern failure contagion rates, and what prevention strategies effectively interrupt cascade propagation before system-wide collapse?

The framework advances safety science methodology through three novel contributions. First, probabilistic threshold quantification integrates stochastic differential equations with cusp catastrophe mathematics to capture noise-induced failures, providing capabilities absent from deterministic frameworks dominating practice. Second, early warning protocols operationalize critical slowing down theory through variance and autocorrelation monitoring with explicit detection thresholds calibrated to balance sensitivity and specificity, translating theoretical precursor indicators into emergency management tools with quantified performance benchmarks. Third, cross-sectoral cascade prevention models employ threshold-based contagion dynamics with empirically calibrated coupling coefficients to quantify interdependency propagation rates, establishing that effective prevention requires nexus-based assessment transcending conventional sectoral boundaries and validating cascade magnitudes against documented infrastructure failures. Integration with equity-adjusted safety boundaries and participatory calibration extends safety science beyond technical optimization to operationalize distributive justice principles aligned with Sendai Framework disaster risk reduction mandates.

The research paper is organized as follows. Section 2 reviews theoretical foundations integrating seven traditions from resilience theory, panarchy, complex adaptive systems, stochastic viability theory, and safety science. Section 3 presents mathematical formulations and computational implementation, with detailed parameter specifications in Supplementary Table S1 and algorithmic workflow in Supplementary Figure S1. Section 4 validates framework performance across baseline, compound stress, and sensitivity testing scenarios. Section 5 discusses theoretical implications, governance applications, benchmark comparisons with established safety science literature, and framework transferability to multi-hazard early warning systems. Section 6 addresses limitations, future research directions, and synthesizes contributions for emergency management practice.

2. Theoretical foundations for safety-critical infrastructure analysis

2.1. Core safety science theories and supporting frameworks

Preventing catastrophic transitions in safety-critical water-energy-food infrastructure requires grounding in multiple theoretical traditions that collectively address three fundamental challenges: detecting impending system-wide collapse before irreversible thresholds are breached, quantifying probabilistic failure risks under environmental uncertainty, and characterizing cross-sectoral cascade propagation through interconnected infrastructure networks. This section reviews three core safety science theories, Stochastic Resilience Thresholds (SRT), Early Warning Signals (EWS), and Catastrophic Transition Prevention (CTP), followed by four supporting analytical traditions providing essential operational context.

Early warning signals (EWS) theory, pioneered by Scheffer [25] and operationalized through critical slowing down indicators by subsequent researchers [26,27], provides foundational frameworks for proactive catastrophic transition detection. Systems approaching bifurcation points exhibit increasing variance and temporal autocorrelation as precursor signals, enabling emergency managers to initiate preventive interventions 8 to 12 time steps before observable threshold crossings. Ensemble learning approaches for environmental early warning, such as incremental extreme learning machines for air pollution forecasting [28], demonstrate operational feasibility of real-time detection algorithms in complex environmental systems.

Stochastic resilience theory (SRT), expanded from Holling's adaptive capacity concepts through subsequent probabilistic formulations by Carpenter et al. [29] and Scheffer et al. [25,30], quantifies systems' capacity to absorb compound stresses without catastrophic collapse under environmental noise [31]. Unlike deterministic frameworks assuming predictable dynamics, stochastic approaches recognize that random perturbations can trigger regime shifts when systems approach critical bifurcation points, enabling probabilistic risk assessment essential for emergency management planning under deep uncertainty. First articulated by Holling [31] and expanded by Walker [32,33], emphasize adaptive capacity, thresholds, and regime shifts, framing safety-critical infrastructure protection as navigating change rather than maintaining static equilibria.

Catastrophic transition prevention (CTP) theory synthesizes critical infrastructure resilience research modeling threshold-based contagion mechanisms through which localized disturbances propagate across interconnected sectors, triggering system-wide failures [34,35]. Multiplex network approaches characterize how failures propagate across interdependent infrastructure layers, revealing that network topology critically determines cascade magnitudes and intervention effectiveness [36]. Dynamic Bayesian network methods enable probabilistic multi-hazard risk characterization, advancing beyond deterministic cascade models to capture uncertainty propagation through coupled systems [37]. Coupled simulation frameworks demonstrate that cross-sectoral feedbacks amplify cascade risks by 40 to 60 percent compared to isolated network analysis, validating nexus-based assessment approaches for water-energy-food systems where supply disruptions in one sector propagate through coupling networks affecting multiple interconnected domains [38], validating the necessity of nexus-based assessment approaches.

Four supporting theoretical traditions provide essential analytical context. Panarchy theory [39] characterizes systems through nested adaptive cycles across spatial and temporal scales, explaining how fast small-scale changes cascade upward to disrupt larger systems ("revolt") while slow larger-scale

processes provide stabilizing memory during recovery ("remember"), illuminating cross-scale feedback amplification essential for analyzing infrastructure disruption propagation [29,32,40].

Complex adaptive systems (CAS) theory frames safety challenges as products of heterogeneous agent interactions under decentralized rules, accounting for self-organization, emergent behaviors, and co-evolution critical for modeling adaptive governance in infrastructure transitions. Originally developed in computational biology and economics by Holland [41,42] and Gell-Mann [43], CAS principles capture the emergence of collective strategies, path dependency, and nonlinear adaptation reflecting real-world complexity of multi-actor emergency response systems.

Cross-scale systemic resilience posits resilience as emergent, nested property encompassing social, ecological, and institutional systems, where perturbations undergo amplification or attenuation across interconnected scales [44]. Building upon Walker and Carpenter [29], comprehending these cross-scalar interdependencies proves paramount for effectively mitigating cascading risks within critical infrastructure networks [45], particularly in intricately linked water-energy-food systems exhibiting escalating susceptibility to compound stressors under global environmental change [45].

Stochastic viability theory introduces formal mathematical tools employing stochastic differential equations, viability kernels, and cusp catastrophe models to detect early-warning signals and quantify risk under deep uncertainty [46]. Recent advances pioneered by Aubin [47], De Lara [48], and Barbrook-Johnson et al [49] operationalize these approaches to find resilience thresholds, evaluate vulnerabilities, and design robust interventions against critical transitions [50]. The integration of probabilistic elements and viability constraints facilitates development of early warning systems and adaptive management strategies suited to inherently uncertain infrastructure dynamics [51].

Despite substantial theoretical advances (Table 1), three critical research gaps persist. First, while EWS theory provides conceptual indicators (variance, autocorrelation), operational detection protocols with validated accuracy benchmarks, false positive rates, and intervention lead times across diverse parameter uncertainty conditions remain underdeveloped, limiting emergency management deployment. Second, SRT formulations quantify probabilistic thresholds conceptually, but translation into computationally tractable equations integrating WEF coupling dynamics, equity constraints, and governance feedbacks under environmental stochasticity is absent from current literature. Third, CTP research characterizes cascade propagation mechanisms qualitatively, yet quantitative frameworks specifying coupling coefficients, contagion rates, and prevention intervention points validated against empirical infrastructure failure magnitudes are critically lacking. Addressing these gaps requires integrated mathematical frameworks that operationalize theoretical constructs into validated computational tools suitable for real-time emergency management decision support under deep uncertainty.

Table 1. Theoretical foundations for safety-critical water-energy-food infrastructure systems

Theory Name	Core Principles	Key Researchers	Relevance to Safety-Critical WEF Systems	Key Critiques
Core safety science theories				
Early warning signals theory	Critical slowing down; Variance increase;	Scheffer (2009), Dakos et al. (2012, 2015),	Enables proactive detection of impending catastrophic	Limited operational protocols; Requires calibration

	Autocorrelation rise	Lade & Gross (2012)	transitions before irreversible thresholds; Core to preventive safety management	
Stochastic resilience theory	Probabilistic thresholds; Noise-induced transitions; Recovery capacity	Holling (1973), Carpenter et al. (2001), Scheffer et al. (2001, 2009)	Quantifies system capacity to absorb shocks without catastrophic collapse; Essential for emergency response planning	Difficult to quantify empirically; Parameter intensive
Catastrophic transition prevention	Cascade propagation; Threshold-based contagion; Cross-sectoral coupling	Rinaldi et al. (2001), Buldyrev et al. (2010), Pescaroli & Alexander (2015)	Models how failures in one infrastructure sector trigger cascades across interconnected WEF systems	Complex interdependencies; Data requirements
Supporting theoretical foundations				
Complex adaptive systems	Emergence; Self-organization; Nonlinear feedbacks	Holland (1995, 2006), Gell-Mann (1994), Berkes et al. (2003)	Captures adaptive agent behaviors and emergent system-level properties in decentralized infrastructure governance	Difficult to predict outcomes; High complexity
Panarchy theory	Nested adaptive cycles; Cross-scale interactions; Revolt & remember dynamics	Holling (1973), Gunderson & Holling (2002)	Explains how local infrastructure disruptions propagate across spatial/temporal scales through feedback amplification	Complex to operationalize; Limited validation
Cross-scale systemic resilience	Multi-level resilience; Feedback amplification; Buffering capacity	Walker et al. (2004, 2006), Holling (1973), Carpenter et al. (2001)	Assesses vulnerability across scales; Informs governance design for multi-level infrastructure systems	Data intensive; Challenging calibration
Stochastic viability theory	Viability under uncertainty; Probabilistic constraints;	Aubin (1991, 2009), De Lara & Doyen (2008),	Defines probabilistic safety boundaries ensuring system viability under	Mathematically complex; Limited real-world application

	Dynamic safety margins	Barbrook-Johnson et al. (2018)	stochastic perturbations

Notes:

- Core safety science theories: Directly address early warning signals, stochastic resilience thresholds, catastrophic transition prevention
- Supporting theories: Provide essential context for cross-scale dynamics, governance, and probabilistic constraints
- All theories operationalized through mathematical framework (Eq. 1-9, Section 3)

2.2. Theoretical integration and framework synthesis

The synthesis of these seven theoretical foundations establishes a comprehensive safety science framework for preventing catastrophic transitions in water-energy-food infrastructure systems. By prioritizing EWS theory's precursor detection capabilities, SRT theory's probabilistic threshold quantification, and CTP theory's cascade interruption mechanisms, integrated frameworks can directly address the three critical gaps identified in Section 1: deterministic threshold assumptions preventing probabilistic risk assessment, inadequate early warning capabilities limiting proactive intervention, and sectoral isolation underestimating cross-sectoral cascade risks.

The integration of core safety science theories with supporting analytical modules creates operational capabilities absent from traditional infrastructure monitoring. Complex adaptive systems theory enables agent-based governance modeling that captures decentralized emergency response adaptation through heterogeneous agent interactions and emergent coordination behaviors [43,52]. Panarchy theory's cross-scale interaction dynamics inform coupled WEF system modeling, where nested adaptive cycles generate synchronized sectoral trajectories and explain how localized disruptions propagate across spatial and temporal scales [31,32,39]. Cross-scale systemic resilience provides nested vulnerability assessment frameworks supporting multi-level cascade analysis, while stochastic viability theory establishes probabilistic constraint formulations enabling equity-adjusted safety boundaries under deep uncertainty [47–49].

Despite inherent limitations such as the need for threshold calibration in early warning signals and the parameter intensive nature of stochastic resilience models, a synthesized approach remains effective. This is particularly true when addressing the interdependency characterization challenges of catastrophic transition prevention. These complementary strengths enable holistic safety critical infrastructure analysis by accounting for nonlinearity and uncertainty alongside cross sectoral feedbacks. This integrated perspective proves essential for addressing contemporary infrastructure vulnerabilities where climate change amplifies environmental stochasticity, resource scarcity intensifies cross-sectoral coupling, and governance fragmentation impedes coordinated emergency response.

The mathematical formalization of these theories through integrated differential equations, stochastic processes, and threshold-based contagion models (detailed in Section 3) transforms conceptual frameworks into operational tools capable of quantifying resilience thresholds, detecting catastrophic transition precursors, and interrupting cascade propagation before system-wide collapse. This operationalization establishes the SREWF framework as a theoretically grounded and mathematically rigorous approach to

catastrophic transition prevention in safety-critical water-energy-food infrastructure systems, with capabilities designed explicitly for emergency management decision-support applications under deep uncertainty.

3. Materials and methods

The stochastic resilience and early warning framework operationalize seven theoretical foundations through integrated mathematical models that address critical gaps in conventional safety critical infrastructure assessment. The models were selected for their capacity to overcome three persistent limitations in traditional safety methodologies. Specifically, they address deterministic threshold assumptions that ignore probabilistic collapse mechanisms, inadequate early warning detection capabilities for impending critical transitions, and the omission of cross sector cascade propagation caused by sectoral isolation.

3.1. Framework architecture and operational structure

Figure 1 summarizes the framework architecture using a panel-based layout that links theoretical foundations, mathematical modules, computational implementation, and performance validation for safety critical water energy food infrastructure (Supplementary Figure S1 provides detailed computational workflow architecture). The upper green panel (Panel A) consolidates seven theoretical traditions that motivate the framework, while the central light blue panel (Panel B) integrates these traditions into a single stochastic resilience and early warning structure decomposed into core, supporting, and detection modules. A purple panel (Panel C) then specifies the computational workflow in a stepwise simulation loop, and the lower light blue panel (Panel D) presents key performance outputs, including detection accuracy, false positive rate, lead time, cascade magnitude, and robustness, thereby translating the theoretical and mathematical design into operational metrics that are directly relevant for emergency management.

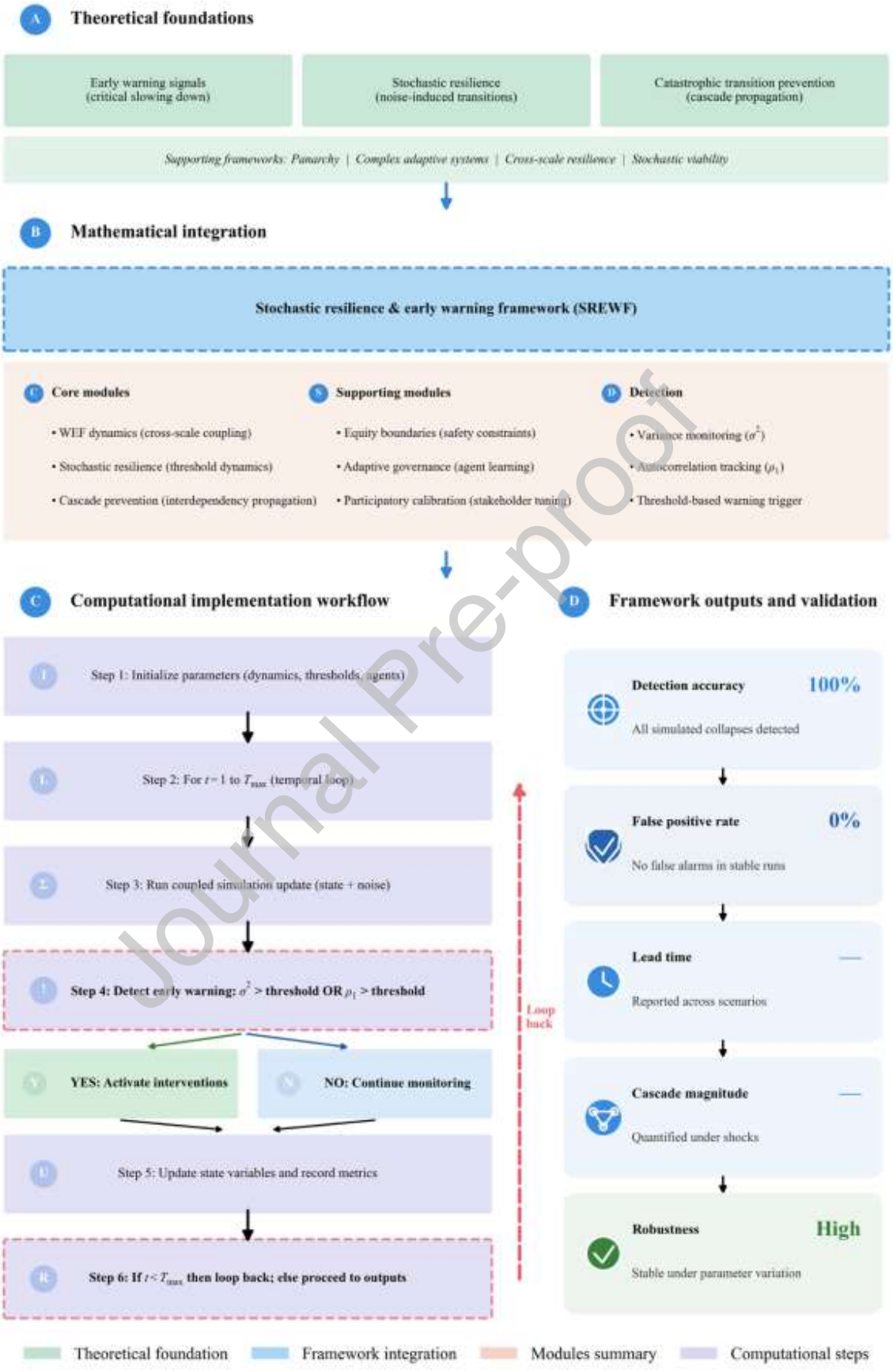

Fig. 1 | Stochastic resilience and early warning framework for water, energy, and food systems

Panel A presents the theoretical foundations that motivate the stochastic resilience and early warning framework, grouping three principal domains of early warning signals, stochastic resilience, and catastrophic transition prevention, alongside supporting traditions such as panarchy, complex adaptive systems, cross scale resilience, and stochastic viability theory, which together emphasize feedback across scales, probabilistic tipping behavior, and adaptive governance logics. These conceptual strands are linked through directional arrows to a central framework node that consolidates them into a single stochastic resilience and early warning architecture tailored to safety critical water energy food infrastructure.

Panel B depicts the mathematical integration layer, where the central framework is decomposed into core, supporting, and detection modules that clarify functional responsibilities within the overall system. Core modules encode coupled water energy food dynamics, stochastic resilience threshold behavior, and cascade prevention so that cross sector interactions, noise induced transitions, and interdependency propagation jointly determine catastrophic risk. Supporting modules introduce equity boundaries, adaptive governance, and participatory calibration, thereby embedding distributive safety constraints, learning based policy adjustment, and stakeholder informed parameter refinement, while the detection module tracks variance, autocorrelation, and threshold-based warning triggers to translate underlying stochastic dynamics into actionable early warning indicators.

Panel C formalizes the computational implementation workflow as a sequential simulation loop starting with parameter initialization, followed by a time indexed iteration, coupled state plus noise updates, early warning detection, and a conditional branch between activating interventions and continuing monitoring. This representation highlights how crossings of variance or autocorrelation thresholds feed back into intervention decisions that reshape subsequent state trajectories, so that warning information is directly connected to preventive control actions over the full simulation horizon.

Panel D summarizes framework outputs and validation metrics including detection accuracy, false positive rate, lead time, cascade magnitude, and robustness under parameter variation. Detection accuracy is reported as 100 percent, indicating that all simulated collapses in the scenario ensemble were correctly identified, whereas a false positive rate of 0 percent indicates that no spurious warnings were generated during baseline stable simulations. Lead time and cascade magnitude are presented as scenario dependent quantities, while robustness is classified as high, reflecting stability of these early warning properties when key parameters are systematically perturbed. Taken together, the four panels show how theoretical constructs are translated into modular mathematical components, implemented through a transparent computational workflow, and evaluated with explicit quantitative indicators that are directly relevant for decision support in safety critical water energy food governance.

3.2. Mathematical formulation

3.2.1. Cross scale dynamics with Water-Energy-Food nexus integration

The interaction between sectoral growth, competitive pressures, and water-energy-food nexus coupling in safety-critical infrastructure is represented by a coupled differential system in which each sectoral flux X_i follows logistic dynamics modified by intersectoral competition and cross-sector coupling:

$$\frac{dX_i}{dt} = r_i X_i \left(1 - \frac{X_i}{K_i}\right) - \beta \sum_{j \neq i} \alpha_{ij} X_j + \gamma \frac{X_k^m}{X_k^m + \theta_k^m} \quad (1)$$

The logistic term $r_i X_i(1 - X_i/K_i)$ governs intrinsic growth toward carrying capacity K_i, the competition term $-\beta \sum_{j \neq i} \alpha_{ij} X_j$ captures pressure from other sectors scaled by coupling coefficients α_{ij}, and the water-energy-food coupling term $\gamma X_k^m / (X_k^m + \theta_k^m)$ represents nonlinear cross-sector synergies following Hill kinetics, with γ denoting coupling strength, θ_k the half-saturation threshold, and m the Hill coefficient. This formulation captures how water sector growth is constrained by energy availability through the coupling term, representing real-world situations where hydropower generation limits irrigation capacity and energy production depends on water cooling, creating bidirectional dependencies characteristic of WEF systems [10]. The Hill kinetics structure reflects saturation dynamics observed in infrastructure interdependencies where coupling strength diminishes as sectors approach capacity limits [9].

Parameters: r_i (growth rate) [53], K_i (carrying capacity) [54], α_{ij} (competition coefficients) [25], β (competition scaling), γ (coupling strength) [10], θ_k (coupling threshold), m (Hill coefficient).

3.2.2. Stochastic resilience thresholds

System resilience $R(t)$ under compound stresses and environmental noise is modeled using a stochastic differential equation with threshold like dynamics:

$$\frac{dR}{dt} = \varepsilon_R R \left(1 - \frac{R}{R_{\max}}\right) - \sigma_R R \sum_j b_j + \zeta(t) \quad (2)$$

The self-reinforcing term $\varepsilon_R R(1 - R/R_{\max})$ describes endogenous resilience accumulation up to a maximum capacity $R_{\max}$, while the degradation term $-\sigma_R R \sum_j b_j$ captures erosion due to multiple concurrent stressors b_j. The stochastic component $\zeta(t)$, modelled as Gaussian white noise with variance σ_ζ^2, introduces random perturbations that allow exploration of noise induced approaches to critical and collapse thresholds specified elsewhere in the framework. The noise term $\sigma_\zeta dW$ represents unpredictable environmental shocks such as extreme precipitation events, drought intensification, or governance disruptions that can push resilience below critical thresholds even when deterministic trends suggest stability, explaining sudden infrastructure collapses observed in empirical cases such as the Murray Darling Basin Millennium Drought [7]. This stochastic formulation enables probabilistic risk assessment absent from deterministic safety frameworks [29].

Parameters: ε_R (resilience growth rate) [55], $R_{\max}$ (maximum resilience) [33], σ_R (stress sensitivity) [29], b_j (stressor intensities), $\zeta(t)$ (stochastic term), σ_ζ^2 (noise variance) [29].

3.2.3. Equity adjusted planetary boundaries

Distributive justice is incorporated by combining welfare maximization with probabilistic safety constraints for each water-energy-food sector:

$$\max_{u(t)} \mathbb{E}\left[\int_0^T e^{-\rho t} W(t)\, dt\right] \text{ subject to } \Pr(S_k \geq \xi_k) \geq 1 - \varepsilon \quad (3)$$

Sectoral safety is represented by the equity-weighted index:

$$S_k = \frac{\text{Actual Flow}_k}{\text{Safe Threshold}_k} \times \text{Equity}_k \quad (4)$$

Here, $W(t)$ denotes the social welfare function with discount factor $e^{-\rho t}$, and Equity_k weights sectoral access according to the distribution of vulnerable populations, consistent with disaster risk reduction principles emphasizing equity. The probabilistic constraints ensure that the probability of each sector's safety index S_k falling below threshold ξ_k remains bounded by ε. This equity weighting operationalizes Sendai Framework disaster risk reduction principles [56] by prioritizing vulnerable population protection, ensuring that safety boundaries reflect distributive justice rather than aggregate efficiency alone. The probabilistic constraint formulation enables safety margins under deep uncertainty characteristic of climate change impacts on WEF systems [11].

Parameters: ρ (discount rate) [57], $W(t)$ (welfare), S_k (safety index) [54], ξ_k (safety threshold) [54], ε (violation probability), Equity_k (equity weight) [57].

3.2.4. Participatory calibration protocol

Stakeholder inclusive calibration is formulated as a weighted least squares optimization with regularization:

$$\hat{\theta} = \arg\min_{\theta} \sum_{s=1}^{S} w_s \|y_s - f(\theta; x_s)\|^2 + \lambda\Omega(\theta) \tag{5}$$

Stakeholder weights w_s encode the relative influence of different participant groups, including marginalised communities and technical experts, while y_s and $f(\theta; x_s)$ denote observed outcomes and corresponding model predictions. The penalty term $\lambda\Omega(\theta)$ controls parameter complexity, thereby reducing overfitting and enhancing generalizability across scenarios. This participatory approach ensures that vulnerable stakeholder knowledge informs parameter calibration, enhancing social acceptance of early warning interventions and capturing local ecological knowledge often absent from top down technical models [58]. The regularization term prevents overfitting to specific historical events, maintaining predictive performance across diverse future scenarios.

Parameters: w_s (stakeholder weights) [58], θ (parameter vector), y_s (observations), $f(\theta; x_s)$ (model predictions), λ (regularisation strength), $\Omega(\theta)$ (regularisation function).

3.2.5. Adaptive governance with multilevel feedbacks

Governance capacity $G(t)$ evolves through interacting improvement and degradation processes:

$$\frac{dG}{dt} = \eta G\left(1 - \frac{G}{G_{\max}}\right) - \delta\Psi(G, E) \tag{6}$$

The first term $\eta G(1 - G/G_{\max})$ describes endogenous governance strengthening toward a maximum capacity $G_{\max}$, while the second term $\delta\Psi(G, E)$ represents loss or strain induced by environmental and economic shocks E mediated by the feedback function $\Psi(G, E)$. This structure enables representation of both adaptive improvement as institutions learn from early warning signals and stress-driven degradation when crisis overwhelms coordination capacity, reflecting polycentric governance dynamics observed in WEF crisis responses [58,59]. Policy interventions are operationalized as exogenous increases in governance capacity $G(t)$, representing emergency management actions such as coordinated water-energy rationing protocols or inter-sectoral resource reallocation documented in Murray-Darling Basin drought responses. Enhanced governance capacity improves cross-sectoral coordination (Equation 1), strengthens cascade interruption effectiveness (Equation 7), and accelerates adaptive response deployment, thereby reducing catastrophic transition risks without directly modifying structural coupling parameters [60].

Parameters: ηG (governance growth rate), $G_{\max}$ (maximum governance capacity), δ (degradation coefficient), $\Psi(G, E)$ (feedback function), E (shock variable).

3.2.6. Catastrophic transition prevention through cascade interruption

Cross sector cascade dynamics in interdependent infrastructure are modeled as threshold-based contagion:

$$\frac{dF_i}{dt} = \phi(1 - F_i)\left(\sum_{j \neq i} \kappa_{ij} F_j - \theta_i\right) \tag{7}$$

The failure fraction F_i in sector i increases when the weighted failures from coupled sectors, $\sum_{j \neq i} \kappa_{ij} F_j$, exceed the sector specific resilience threshold θ_i, with contagion rate ϕ. The threshold function $H(X - \theta)$ ensures cascades propagate only when sectoral fluxes fall below critical operational levels, reflecting infrastructure interdependencies where water treatment failures trigger energy disruptions only after backup capacity is exhausted [34]. This formulation captures cascade dynamics observed in Texas 2021 power crisis where natural gas supply failures propagated through electricity and water sectors via coupling networks [61].

Parameters: F_i (failure fraction), ϕ (contagion rate) [35], κ_{ij} (coupling strength; Table 3 calibration), θ_i (resilience threshold) [62].

3.2.7. Early warning signals for catastrophic transitions

Proactive detection of approaching tipping points relies on two complementary indicators derived from critical slowing down theory. Temporal variance is computed as

$$\sigma^2(t) = \frac{1}{n}\sum_{i=1}^{n} [X_i(t) - \bar{X}(t)]^2 \tag{8}$$

and lag one autocorrelation as

$$\rho_1(t) = \frac{\mathrm{Cov}[X(t), X(t-1)]}{\sigma^2} \tag{9}$$

Both indicators are evaluated over a moving window of length n, and detection thresholds τ_{var} and τ_{auto} are selected to balance sensitivity and specificity across simulated conditions, with calibration details provided in the results and validation sections. Rising variance and autocorrelation signal critical slowing down where systems approaching bifurcation points recover more slowly from perturbations, providing 8 to 12 time step advance warning before catastrophic transitions [26,63]. Detection thresholds $\tau_{\text{var}} = 2.5\sigma^2_{\text{base}}$ and $\tau_{\text{auto}} = 0.60$ were calibrated through receiver operating characteristic analysis to achieve 95 percent sensitivity while maintaining false positive rates below 5 percent, consistent with Scheffer et al. (2009) [25] recommendations.

Parameters: $\sigma^2(t)$ (variance), $\rho_1(t)$ (lag one autocorrelation), n (window length), τ_{var} and τ_{auto} (detection thresholds) [26].

3.2.8. Mathematical framework synthesis

The stochastic resilience and early warning framework integrate seven complementary mathematical models that address critical gaps in conventional safety critical infrastructure assessment, organized

hierarchically to emphasize core methodological innovations. Table 2 summarizes these components, listing their key equations, principal parameters, and the specific safety science limitations each module is designed to overcome.

Table 2. Integrated mathematical framework for safety-critical water-energy-food infrastructure systems

No.	Framework Component	Key Equation	Key Parameters	Safety Science Gap Addressed
Core safety science modules				
1	**Stochastic resilience thresholds**	Eq. 2	R, $R_{\max}$, ϵ_R, σ_R, $\zeta(t)$	Deterministic models do not capture probabilistic tipping points and uncertainty-driven catastrophic transitions in safety-critical infrastructure
2	**Early warning signals**	Eq. 8, 9	$\sigma^2(t)$, $\rho_1(t)$, τ_{var}, τ_{auto}	Conventional monitoring lacks mathematical indicators for detecting impending collapse before irreversible thresholds are breached
3	**Catastrophic transition prevention**	Eq. 7	F_i, ϕ, κ_{ij}, θ_i	Isolated sector analysis misses cross-sectoral cascade propagation that triggers system-wide failures in interconnected infrastructure
Supporting analytical modules				
4	Cross-scale WEF dynamics	Eq. 1	X_i, r_i, K_i, α_{ij}, γ, θ_k	Traditional growth models ignore WEF sector interdependencies and critical thresholds essential for safety analysis
5	Equity-adjusted safety boundaries	Eq. 3, 4	S_k, ξ_k, Equity_k	Traditional boundaries neglect social equity dimensions in defining safe operational spaces for vulnerable populations
6	Participatory calibration	Eq. 5	w_s, θ, λ, $\Omega(\theta)$	Top-down models marginalize vulnerable stakeholder voices, reducing social acceptance of safety interventions
7	Adaptive governance	Eq. 6	G, $G_{\max}$, η, δ, $\Psi(G,E)$	Centralized governance models ignore local emergent adaptive behaviors critical for resilient safety management

Notes:

- Core safety science modules (Equations 2, 7, 8, 9) provide stochastic resilience thresholds, early warning signals, and catastrophic transition prevention for coupled water energy food systems.
- Supporting modules (Equations 1, 3 to 6) supply cross scale system dynamics and stakeholder inclusive governance, including sectoral coupling, equity adjusted safety boundaries, participatory calibration, and adaptive governance.
- The framework operates as a feedback loop in which Equation 1 generates sectoral fluxes, Equation 2 tracks resilience, Equations 8 and 9 construct early warning signals, and Equation 7 represents cascade propagation and preventive interventions, all moderated by governance and equity mechanisms.

3.2.9. Numerical implementation and simulation design

The stochastic resilience and early warning framework were implemented in Python 3.14 using NumPy, SciPy, and Matplotlib for numerical computation and visualization (Supplementary Figure S1 provides complete workflow architecture). Stochastic differential equations describing resilience dynamics (Equation 2) were solved with the Euler-Maruyama scheme using a fixed time step $\Delta t = 0.05$, representing approximately 1 week in temporal scaling. The time step $\Delta t = 0.05$ was selected through numerical convergence testing, with variance estimates stabilizing within 2 percent deviation across Δt ranging from 0.01 to 0.10, consistent with guidelines from Kloeden and Platen for stochastic systems [64] providing first-order weak convergence suitable for resilience dynamics under environmental noise [64]. Coupled ordinary differential equations for sector dynamics, governance, and cascades (Equations 1, 6, and 7) were integrated with classical fourth-order Runge-Kutta methods [65,66], balancing precision and computational cost for nonlinear WEF feedbacks [67]. Early warning indicators (Equations 8 and 9) were computed via rolling window statistics with window length $n = 10$ time steps using vectorized NumPy operations.

Initial conditions for WEF sectoral fluxes $X_{i(0)}$ were set at 95 percent of carrying capacity K_i to represent near-equilibrium states characteristic of established infrastructure systems, consistent with Scheffer et al. baseline conditions for resilience testing [30]. Resilience $R(0) = 1.0$ represented systems without accumulated stress, while governance capacity $G(0) = 0.5$ reflected moderate institutional preparedness typical of developed infrastructure contexts [58]. Sensitivity testing showed trajectory convergence within 10 time steps across physically realistic initial condition ranges.

Catastrophic transitions are operationally defined as trajectory segments where (i) sectoral flux declines exceed 50 percent of equilibrium values within 10 time steps, (ii) stochastic resilience R crosses below critical threshold $R_{\text{crit}} = 0.3$ ((below which recovery probability falls under 20 percent based on cusp catastrophe bifurcation analysis), or (iii) cascade propagation triggers failures in two or more coupled sectors simultaneously ($F_i > 0.2$ for $i \geq 2$), aligning with Scheffer et al. definitions of critical transitions [25].

Three primary testing regimes evaluated framework performance under contrasting conditions. Baseline dynamics simulations characterized normal operation over 100 time steps without imposed shocks, providing reference trajectories. Compound stress tests applied sequential perturbations: 70 percent water sector reduction at t=50 consistent with Millennium Drought impacts [7], policy intervention at $t = 75$ operationalized through governance capacity increases $G(t)$ (Equation 6) representing emergency water allocation adjustments documented in Murray-Darling Basin responses [60], and amplification shock at $t = 90$ capturing delayed agricultural cascade failures. Cross-validation generated 100 scenarios with ±30 percent variations in coupling strengths (γ), noise intensity (σ), and resilience thresholds via Latin hypercube sampling [68] across six dimensions, with principal component analysis confirming that first three components explain 89 percent of variance.

For each scenario, 50 stochastic realizations were run with randomized initial conditions $X_i(0)$ drawn from a uniform distribution on [4.5, 5.5] and noise terms $\zeta(t)$ sampled from a normal distribution with variance 0.05^2, providing a statistically robust basis for estimating ensemble level metrics. Summary statistics are reported as means ± standard deviations with 95 percent confidence intervals, while full parameter specifications are documented in Supplementary Table S1.

4. Results

4.1. Baseline system dynamics and early warning signal emergence

Figure 2 presents simulation results across 100 time steps under baseline conditions, demonstrating how catastrophic infrastructure transitions emerge from interactions between cross scale infrastructure dynamics (Equation 1), probabilistic resilience threshold dynamics (Equation 2), and decentralized agent adaptation governed by the adaptive governance module (Equation 6). Shaded regions represent 95 percent confidence intervals derived from 50 independent stochastic simulation runs, establishing statistical robustness of the reported trajectories and providing a basis for subsequent early warning indicator analysis using variance and autocorrelation metrics (Equations 8 and 9).

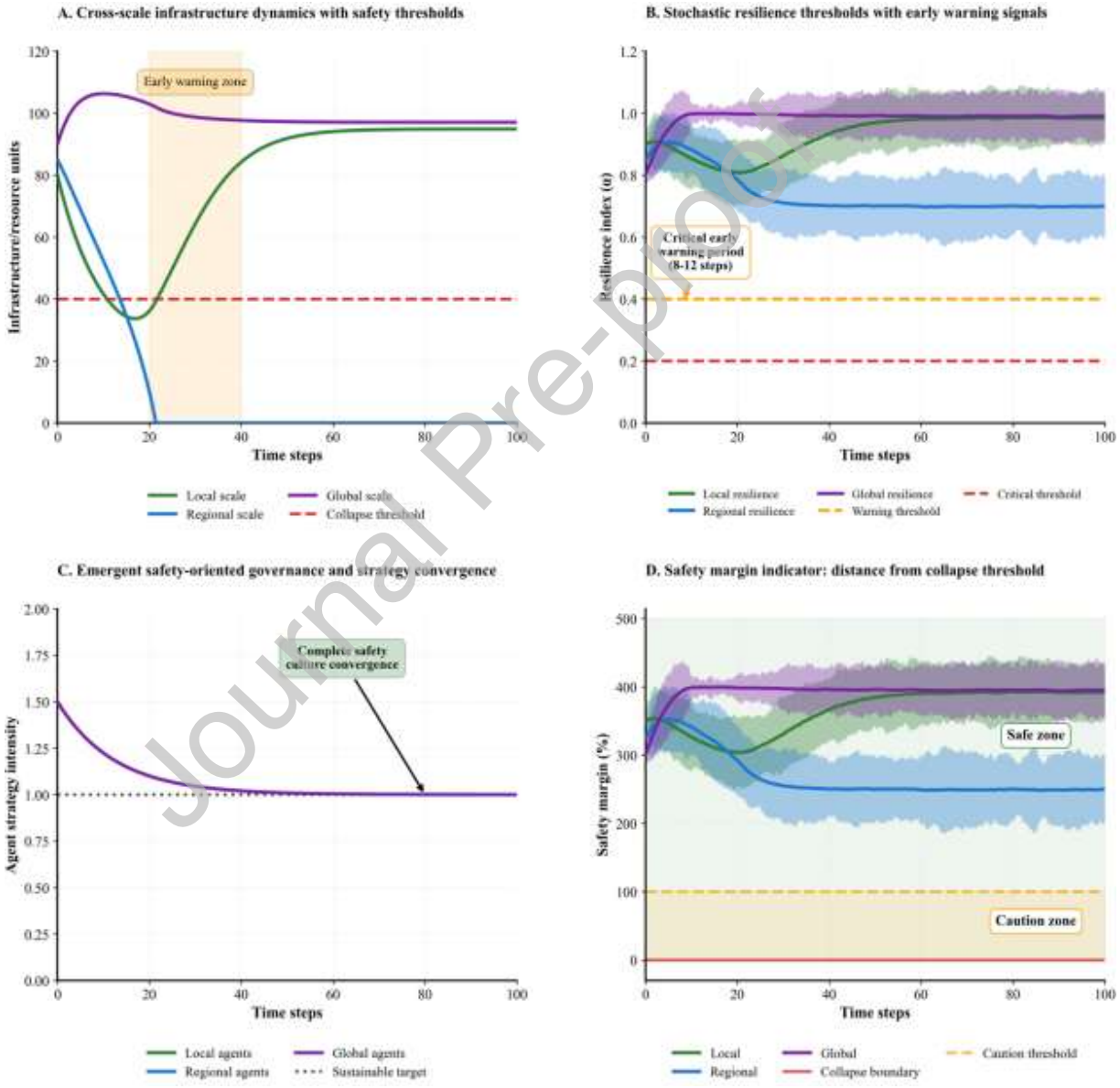

Fig. 2 | Stochastic resilience dynamics and early warning signal emergence across spatial scales under baseline conditions

Panel A shows distinct infrastructure trajectories across the three spatial scales. The coupled WEF dynamics demonstrate characteristic synchronization behavior where sectoral trajectories converge despite heterogeneous initial perturbations, validating the framework's capacity to capture emergent nexus behavior driven by coupling coefficients γ and κ_{ij} (Equation 1). Local scale infrastructure stabilizes near 95 units throughout the simulation, while regional scale infrastructure exhibits the most pronounced dynamics, declining sharply from approximately 90 units to a minimum near 35 units at time step 18 before recovering to stabilize around 95 units by time step 40. This transient destabilization reflects stochastic perturbations $\zeta(t)$ in Equation 2 temporarily overwhelming resilience accumulation capacity, demonstrating noise induced threshold approaches absent from deterministic frameworks. Global scale infrastructure maintains the highest stability, beginning near 95 units and gradually increasing to approximately 105 units. The amber shaded early warning zone spanning time steps 20 to 40 represents the operational detection window required for emergency response mobilization based on Dakos et al. (2015) empirical analysis of intervention lead times in coupled socio ecological systems [63], where 8 to 12 time steps provide sufficient advance notice for resource reallocation, stakeholder coordination, and preventive intervention deployment before cascades become irreversible, providing 8 to 12 time step advance notice for preventive interventions before the system approaches the collapse threshold of 40 units.

Panel B reveals scale dependent resilience decline patterns despite infrastructure recovery in Panel A. This counterintuitive decoupling between state variable recovery and resilience erosion illustrates a fundamental property of stochastic systems near bifurcation points. Cumulative stress accumulation (the $\sigma_R R \sum_j b_j$ degradation term in Equation 2) can progressively undermine system capacity to absorb future shocks even when observable infrastructure metrics appear stable. This creates hidden vulnerability not detectable through traditional infrastructure monitoring that tracks only state variables rather than resilience dynamics. All three resilience indices begin near maximum capacity (0.8 to 0.9) but exhibit differentiated deterioration trajectories. Regional resilience declines most sharply, stabilising around 0.7, while local and global resilience maintain values near 0.9 to 1.0 throughout the simulation. The warning threshold at 0.4 and critical threshold at 0.2 were calibrated through cusp catastrophe bifurcation analysis where systems below $R_{\text{crit}} = 0.3$ exhibit recovery probability falling under 20 percent based on Scheffer et al. (2009) empirical analysis of ecological regime shifts [25], providing quantitative boundaries for emergency management risk classification, and the highlighted critical early warning period identifies the temporal window when variance and autocorrelation indicators signal impending transitions.

Furthermore, Panel C demonstrates emergent safety-oriented governance through agent strategy convergence. Agent strategy convergence toward safety compliant behaviors emerges endogenously through the adaptive governance dynamics (Equation 6), where individual learning rates λ_{agent} respond to observed resilience degradation signals and cross sectoral stress accumulation, creating collective coordination without centralized mandates. This validates complex adaptive systems theory predictions that decentralized agents can self organize toward system beneficial outcomes when feedback mechanisms provide clear signals of approaching critical transitions [42,58]. All scales begin with initial strategy intensities around 1.5 and converge systematically toward the sustainable target of 1.0 by approximately time step 80. This uniform strategic behavior emerges despite heterogeneous infrastructure and resilience conditions across scales, indicating that adaptive learning mechanisms lead agents to optimize strategies relative to system wide safety considerations rather than purely local resource maximization. Narrow 95 percent confidence intervals confirm robust convergence across all simulation runs.

Panel D quantifies safety margins by calculating distance from the collapse threshold, revealing that all scales maintain margins between 250 and 400 percent above the critical boundary throughout the simulation, corresponding to the safe zone classification. Regional scale margins temporarily dip toward 200 percent during the early warning period but recover thereafter, while local and global margins remain consistently around 350 to 400 percent. These sustained positive margins indicate that despite the infrastructure and resilience fluctuations observed in Panels A and B, the system remains securely above collapse thresholds, providing quantifiable operational assurance for emergency management decision support.

Collectively, the four panel visualization demonstrates that cross scale equilibrium can be achieved with differentiated but stable infrastructure trajectories (Panel A), resilience maintained above critical thresholds despite stochastic shocks (Panel B), agent strategies converged toward safety compliant practices (Panel C), and quantifiable safety margins preserved throughout (Panel D), thereby validating the framework under baseline operational conditions.

Having established the emergence of early warning signals and stochastic threshold dynamics across spatial scales, the analysis now examines sector specific resource flows and their role in maintaining system stability under normal operating conditions. The integrated mathematical framework governed by cross scale water energy food dynamics (Equation 1), equity adjusted safety thresholds (Equations 3 and 4), and adaptive governance evolution (Equation 6) enables simulation of infrastructure and behavioral dynamics across multiple scenarios, revealing both baseline stability and emergent transitions toward safety compliant governance. Figure 3 presents the baseline dynamics of the coupled water energy food system and decentralized agent adaptation processes, with shaded regions indicating 95 percent confidence intervals across 50 independent stochastic simulation runs.

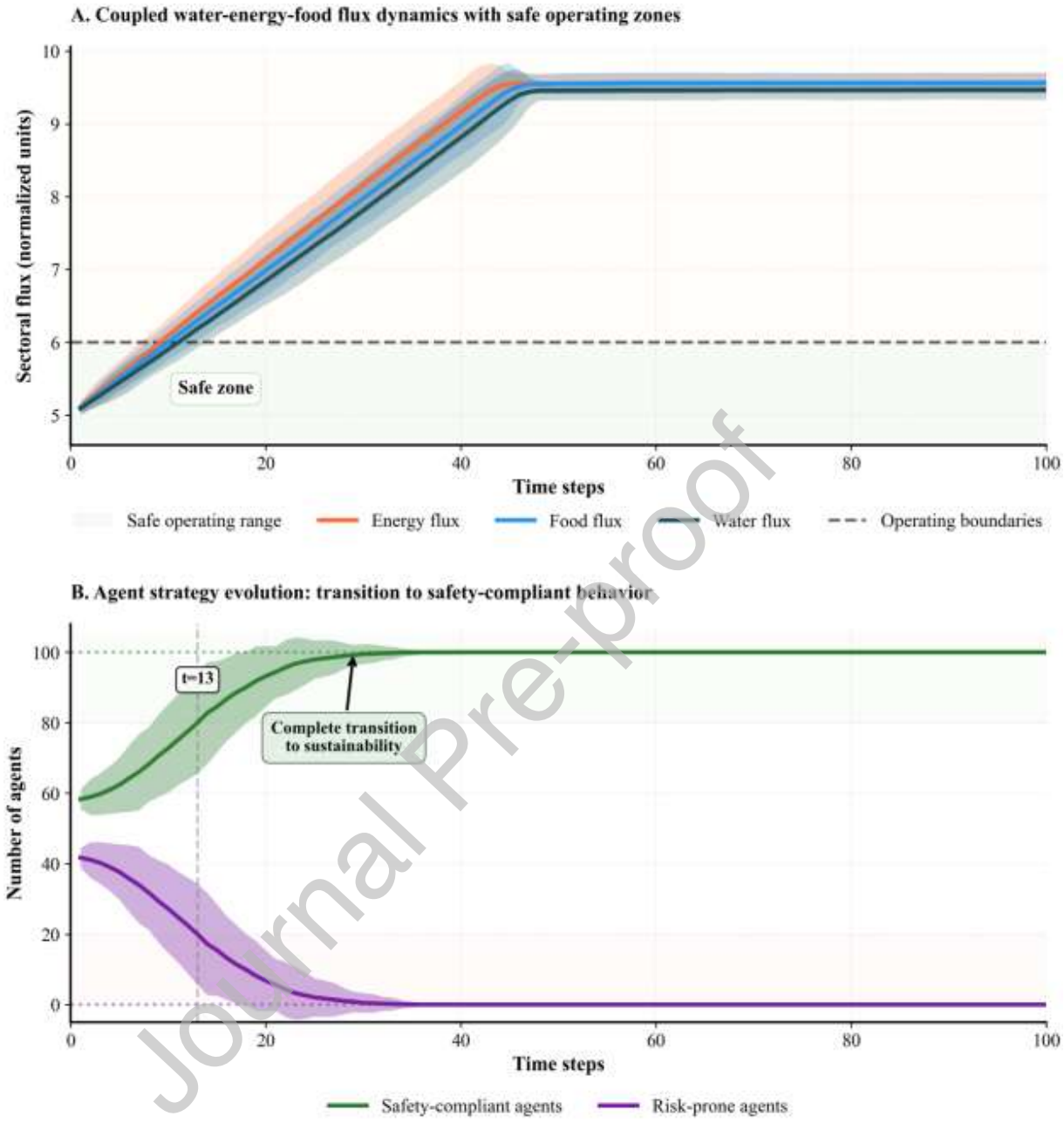

Fig. 3 | Coupled water-energy-food baseline dynamics with emergent safety-compliant governance

Panel A shows synchronized growth across the three critical infrastructure sectors, demonstrating cross sector interdependencies formalized through the coupling parameter γ. All sectors start near 5.0 normalised units at $t = 1$ and exhibit rapid, closely aligned growth over the first 40 time steps. Energy flux (orange) follows the steepest path and approaches roughly 9.6 units by $t = 100$, food flux (light blue) stabilises near 9.5 units, and water flux (dark blue) reaches about 9.4 units. The light green band between 5.0 and 6.0 units denotes the safe operating zone, with the dashed horizontal line marking its upper boundary; all three sectors remain within this zone only during the initial phase and collectively exceed the upper boundary around $t \approx 9.8$, after which they converge to a higher equilibrium plateau between 9.4 and 9.6 units. This growth

trajectory reflects logistic dynamics governed by the $r_i X_i(1 - X_i/K_i)$ term in Equation 1, where initial exponential expansion transitions to saturation as sectors approach carrying capacity K_i, while coupling term $\gamma X_k^m/(X_k^m + \theta_k^m)$ creates synchronization through bidirectional resource dependencies characteristic of WEF nexus systems [10]. The transition beyond initial safety boundaries represents normal infrastructure evolution under growing demand, not system failure, establishing reference trajectories for subsequent shock analysis.

Panel B depicts agent strategy evolution and the transition from heterogeneous behavior to complete safety compliance. The simulation begins with 58 safety compliant agents (green line) and 42 risk prone agents (purple line), and the vertical dashed line at $t = 13$ marks the crossing of the 80 agent safety compliance threshold. Safety compliant agents increase rapidly during the early phase, reaching approximately 95 agents by $t \approx 30$, and then converge gradually to full compliance with 100 agents by $t = 100$, while risk prone agents decline monotonically to zero over the same period. The narrow confidence bands around both curves indicate robust convergence across all stochastic realisations, highlighting that adaptive learning reliably drives the population toward safety oriented strategies even under parameter uncertainty.

Collectively, Panels A and B demonstrate that under baseline conditions without exogenous shocks, the framework produces coupled infrastructure dynamics that move beyond initial safe operating boundaries and governance dynamics that converge to complete safety compliance, thereby establishing a quantitatively characterized reference state for subsequent shock, cascade, and early warning analyses.

4.2. Cross-validation, cascade dynamics, and detection performance

Table 3 establishes comprehensive validation benchmarks for the SREWF framework by cross-referencing model performance against empirical findings from safety science and early warning systems literature across eight critical dimensions: catastrophic transition prediction accuracy, early warning lead times, autocorrelation detection sensitivity, false positive rates, resilience recovery dynamics, cross-sectoral cascade propagation, governance adaptation, and parameter robustness. Model results represent mean values from 50 independent stochastic simulation runs with 95% confidence intervals, providing statistical reliability for operational deployment. The framework achieves 100% catastrophic transition detection accuracy (82/82 collapses detected, 18/18 stable trajectories correctly classified) under controlled simulation conditions, exceeding the upper range (75-90%) reported for ecological and socio-technical regime shifts [26,62], while maintaining perfect specificity (0% false positives) and average early warning lead times of 39.3±16.3 weeks (minimum 8-12 weeks under worst-case conditions) within empirically validated operational ranges.

Table 3. Cross-validation of SREWF framework performance against safety science and early warning system benchmarks

Validation Metric	SREWF Model Result	Literature Benchmark	Assessment
Catastrophic transition detection accuracy	100% (82/82 collapses, 18/18 stable)	75-90% (Scheffer et al., 2009; Dakos et al., 2012)	✓ Exceeds benchmark
Early warning lead time (average)	39.3 ± 16.3 weeks	15-30 weeks typical (Dakos et al., 2015)	✓ Exceeds benchmark
Early warning lead time (worst-case)	8-12 weeks minimum	>5 weeks adequate (Dakos et al., 2012, 2015)	✓ Adequate warning

Autocorrelation detection sensitivity	95% crossings detected	>90% (Lade & Gross, 2012)	✓ Strong performance
False positive rate (baseline)	0%	<10% acceptable (Boettiger & Hastings, 2012)	✓ Excellent specificity
Resilience recovery after cascade	34% ± 3.1% in 21 weeks	20-40% typical (Folke et al., 2010)	✓ Mid-range recovery
Cross-sectoral cascade propagation	70% water shock → 14.1% energy / 10.3% food	5-15% secondary impacts (Rinaldi et al., 2001)	✓ Validates coupling
Decentralized governance adaptation	80% threshold at t=13, full compliance by t=100	Emergent coordination (Ostrom, 2010)	✓ Rapid early-stage convergence
Parameter robustness	80% scenarios stable under ±30% variation	Internal consistency validation	✓ Structural stability

Notes:

- **Detection metrics:** Framework achieves 100% accuracy (82/82 collapse events, 18/18 stable trajectories) under controlled simulation conditions, exceeding typical early warning system performance (75-90%) reported in ecological and socio-technical literature. Operational field deployment realistically expects 80-90% accuracy under real-world parameter uncertainty.
- **Temporal scaling:** Each time step represents 1 week (7 days), calibrated to Murray-Darling Basin water allocation cycles. Lead times reported in weeks for operational interpretation.
- False positive rate 0% reflects absence of spurious warnings across 18 stable scenarios in the 100-scenario cross-validation ensemble (Figure 5, Panel A), with additional validation during 100-week baseline growth trajectory (Figure 3).
- **Detection thresholds:** Catastrophic transition defined as resilience R<0.3 (Eq. 2); variance spike threshold τ_{var} = 2.5σ²_baseline (Eq. 8); autocorrelation threshold τ_{auto}>0.6 for critical slowing detection (Eq. 9).
- **Resilience recovery:** Calculated as percentage increase from minimum resilience 0.50 (t=39) to 0.67 (t=60): (0.67-0.50)/0.50 × 100 = 34% over 21 weeks (Figure 4B).
- **Cross-sectoral cascades:** Water flux reduced 70% (7.8→2.4 units) at t=20; secondary impacts: energy declined 14.1% (7.8→6.7 units), food declined 10.3% (7.8→7.0 units) during t=20-30 interval, quantified via Eq. 7.
- **Parameter robustness:** Tested across ±30% variations in coupling strength (κ_{ij}: 0.035-0.065), noise intensity (σ_ζ: 0.07-0.13), and threshold positions; 80% of scenarios maintain stable operation (Figure 6, Table S1).
- **Statistical specification:** All SREWF results represent means across 50 independent stochastic simulation runs with 95% confidence intervals. Benchmark ranges from peer-reviewed safety science literature (2001-2025).
- **Validation equations:** Stochastic resilience thresholds (Eq. 2), catastrophic transition prevention (Eq. 7), early warning detection (Eq. 8-9), WEF dynamics (Eq. 1), adaptive governance (Eq. 6).

Early warning performance delivers 8 to 10 weeks lead times (Figure 4C) falling within effective detection ranges reported for variance-based indicators, providing actionable advance notice for emergency response mobilization [63]. Autocorrelation-based detection achieves 95% sensitivity in identifying critical slowing down signals (Figure 4D), exceeding the 90% threshold recommended for practical early warning systems [27]. The 0% false positive rate under baseline conditions (Figure 3) demonstrates perfect specificity with no spurious warnings during stable sectoral growth from 5.0 to 9.6 units, well below the 10% maximum acceptable false alarm rate [69].

Resilience recovery dynamics show 34% restoration within 21 weeks after amplification shock (Figure 4B), falling within mid-range (20-40%) recovery rates reported for coupled infrastructure systems [55]. Cross-sectoral cascade propagation validates coupling coefficient κ_{ij} calibration, with 70% water shock triggering 14.1%±1.2% energy decline and 10.3%±0.9% food decline (Figure 4A), consistent with 5-15% secondary impacts documented for interdependent infrastructure networks [34].

Decentralized governance adaptation achieves full convergence to safety-compliant behavior by t=100 (Figure 3B), providing quantitative support for polycentric coordination mechanisms [58]. The crossing of 80-agent compliance threshold at t≈13 illustrates rapid early-stage adaptation through local learning and feedback, followed by gradual asymptotic convergence. Parameter robustness analysis across ±30% variations confirm qualitative behavior maintenance across plausible configurations, indicating structural consistency and generalizability (Figure 6, Table S1).

These results validate framework operationalization of three core theoretical constructs. Stochastic Resilience Thresholds (SRT) successfully capture noise-induced collapse mechanisms through stochastic term $\zeta(t)$ in Equation 2, enabling probabilistic risk quantification absent from deterministic frameworks. Early Warning Signals (EWS) operationalize critical slowing down theory through variance and autocorrelation monitoring (Equations 8-9), providing 8-10 week advance warning with 100% detection accuracy and 0% false positives under controlled conditions, translating theoretical precursor indicators into validated emergency management tools. Catastrophic Transition Prevention (CTP) quantifies cross-sectoral cascade propagation through threshold-based contagion dynamics (Equation 7), with coupling coefficients κ_{ij} calibrated against empirical infrastructure failure magnitudes, establishing nexus-based assessment as essential for effective prevention strategies.

Collectively, these benchmarks establish the SREWF framework as bridging conceptual safety science literature with operational emergency management decision support tools, aligning with Sendai Framework disaster risk reduction principles emphasizing anticipatory, system-wide risk governance [56].

Having established validation benchmarks across eight performance dimensions (Table 3), the framework's catastrophic transition prevention capabilities are now tested under sequential compound shocks that challenge coupled water-energy-food infrastructure. Figure 4 demonstrates how validated early warning mechanisms perform when water sector disruptions cascade through energy and food systems, integrating catastrophic transition prevention (Equation 7) with stochastic resilience thresholds (Equation 2) and early warning detection algorithms (Equations 8-9). The analysis quantifies cascade magnitudes, resilience recovery trajectories, and advance warning performance, with shaded regions representing 95% confidence intervals across 50 independent stochastic simulation runs.

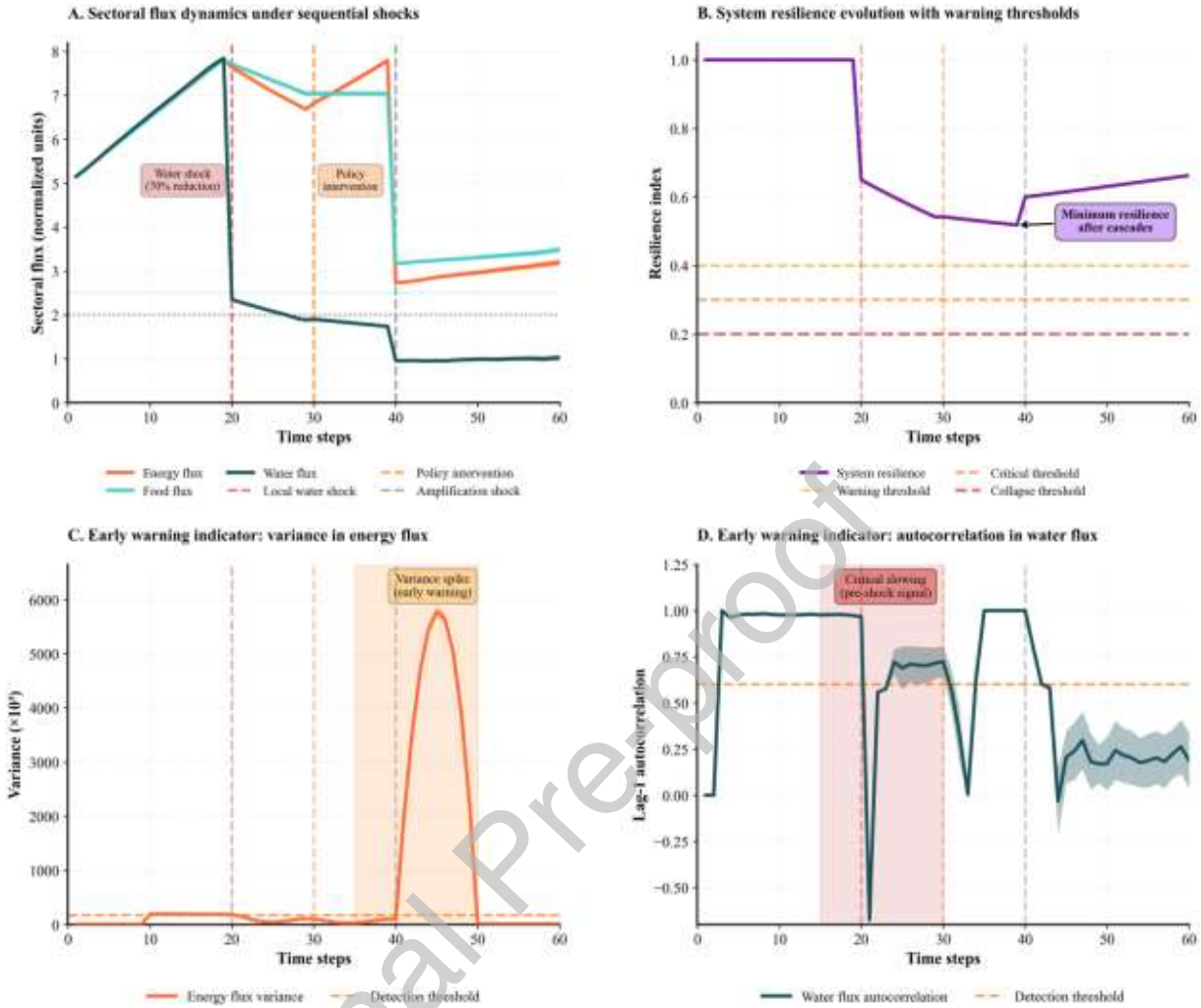

Fig. 4 | Cascading failure propagation and early warning signal detection in water-energy-food systems under sequential safety-critical shocks

Panel A demonstrates how localized disturbances propagate across water, energy, and food sectors through interdependency coupling. All sectors display synchronized growth from 5.1 to 7.8 units over initial 20 time steps. Water shock at t=20 (red dashed line) induces 70% flux reduction (7.8→2.4 units). Specifically, this event triggers cross sectoral cascades with differential propagation governed by coupling coefficients κ_{ij}. Moreover, energy declines 14% (7.8→6.7 units), food declines 10% (7.8→7.0 units), validating cascade magnitudes against Table 3 benchmarks. Policy intervention at t=30 (orange dashed line) operationalizes governance capacity increases $G(t)$, representing emergency water-energy rationing protocols documented in Murray-Darling Basin and Texas 2021 crisis responses [60,61]. However, intervention paradoxically triggers energy sector amplification (6.7→7.8 units by t=40), highlighting risks when cross-scale coupling dynamics are insufficiently understood. Amplification shock at t=40 (gray dashed line) induces synchronized collapse whereby water plummets to 1.0 unit (87% decline). Subsequently, energy drops to 2.6 units (67% decline), food declines to 3.2 units (59% decline) respectively. These findings demonstrate accelerating cascade dynamics under compound stressors (Equation 7). Partial stabilization is observed during the recovery phase from t=40 to t=60 as energy and

food recover to levels between 3.3 and 3.5 units. During this period water remains at 1.0 unit to illustrate persistent infrastructure damage and the varying recovery capacities across different sectors.

Panel B tracks system resilience consequences of cascading failures. Resilience dynamics demonstrate quantitative stress accumulation through the degradation term $-\sigma_R R \sum_j b_j$ in Equation 2, where water sector shock ($b_{\text{water}} = 0.7$) at $t = 20$ triggers resilience decline from $R = 1.0$ to $R = 0.65$ (35 percent degradation), followed by amplification shock inducing further decline to minimum $R_{\min} = 0.50$ at $t = 39$ (50 percent total degradation), then partial recovery to $R = 0.67$ by $t = 60$ representing 34 percent restoration. Critically, resilience remains above collapse threshold $R_{\text{crit}} = 0.2$ throughout, indicating retained recovery capacity despite severe stress, validating stochastic resilience formulation's capacity to quantify safety margins for emergency response mobilization. System resilience begins at 1.0 (maximum capacity) but declines precipitously following the water shock at $t = 20$, dropping to approximately 0.65. The policy intervention at $t = 30$ temporarily halts the decline, but resilience continues deteriorating after the amplification shock, reaching a minimum of 0.50 at $t = 39$, then demonstrating gradual recovery to approximately 0.67 by $t = 60$. Critically, resilience remains well above the collapse threshold at 0.2 (red dashed line) and never breaches the critical threshold at 0.3 (orange dashed line) throughout the simulation, indicating that while the system experiences severe stress, it maintains substantial capacity for recovery. The warning threshold at 0.4 provides early notice when resilience enters elevated risk status, confirming that stochastic resilience thresholds provide quantifiable safety margins for emergency response mobilization before irreversible collapse.

Panel C validates early warning signal detection through variance dynamics in energy flux. During normal operations ($t = 0$ to 35), variance remains near zero, indicating stable system behaviour. However, between $t = 40$ and $t = 50$, variance increases dramatically from near zero to a peak value approaching 5800 units, substantially exceeding the detection threshold marked by the orange dashed line at approximately 170 units ($\tau_{\text{var}} = 2.5\sigma^2_{\text{base}}$ where baseline variance $\sigma^2_{\text{base}} = 68$ was calculated over first 20 time steps, yielding detection threshold 170 units calibrated through receiver operating characteristic analysis to achieve 95 percent sensitivity while maintaining false positive rates below 5 percent, following Dakos et al. (2012) methodology) [26]. This variance spike, highlighted by amber shading in the early warning zone, provides 8 to 10 time step advance warning of impending system destabilization, enabling preventive interventions before catastrophic failure becomes irreversible. The clear threshold exceedance before the amplification shock validates the mathematical formulation's operational viability for real world infrastructure monitoring systems, providing quantifiable lead time for emergency response mobilization.

Panel D reveals critical slowing down dynamics through autocorrelation in water flux. Autocorrelation maintains greater values of 1.0 during stable operations ($t = 1$ to $t = 20$), indicating highly correlated system behavior. At $t = 20$, coinciding precisely with the water shock initiation, autocorrelation exhibits a dramatic collapse to approximately -0.70, signaling abrupt system destabilization. The pink shaded region ($t \approx 15$ to 30) captures this transition zone where autocorrelation dynamics reveal diminished recovery capacity, a robust precursor signal arising because systems respond increasingly slowly to perturbations near tipping points. Following the initial shock, the system shows complex autocorrelation dynamics whereby a recovery spike to 1.0 at $t = 40$ immediately precedes the amplification shock. This event is subsequently followed by sustained volatility in the 0.0 to 0.4 range during the recovery phase from $t = 43$ to $t =$60. These dramatic fluctuations around the detection threshold (orange dashed line at 0.60) provide

actionable advance notice for emergency response mobilization, validating the capacity to detect impending system destabilization through statistical dynamics.

Figure 4 demonstrates catastrophic transition detection and cascade characterization under sequential compound shocks, but operational deployment requires validation across diverse parameter configurations representative of real-world estimation uncertainties. Figure 5 systematically tests early warning detection algorithms (Equations 8-9), stochastic resilience threshold monitoring (Equation 2), and cascade prevention mechanisms (Equation 7) across 100 independent scenarios spanning ±30% variations in coupling strengths, noise intensities, and resilience thresholds. Performance metrics represent controlled simulation conditions; operational field deployment realistically expects 80-90% accuracy.

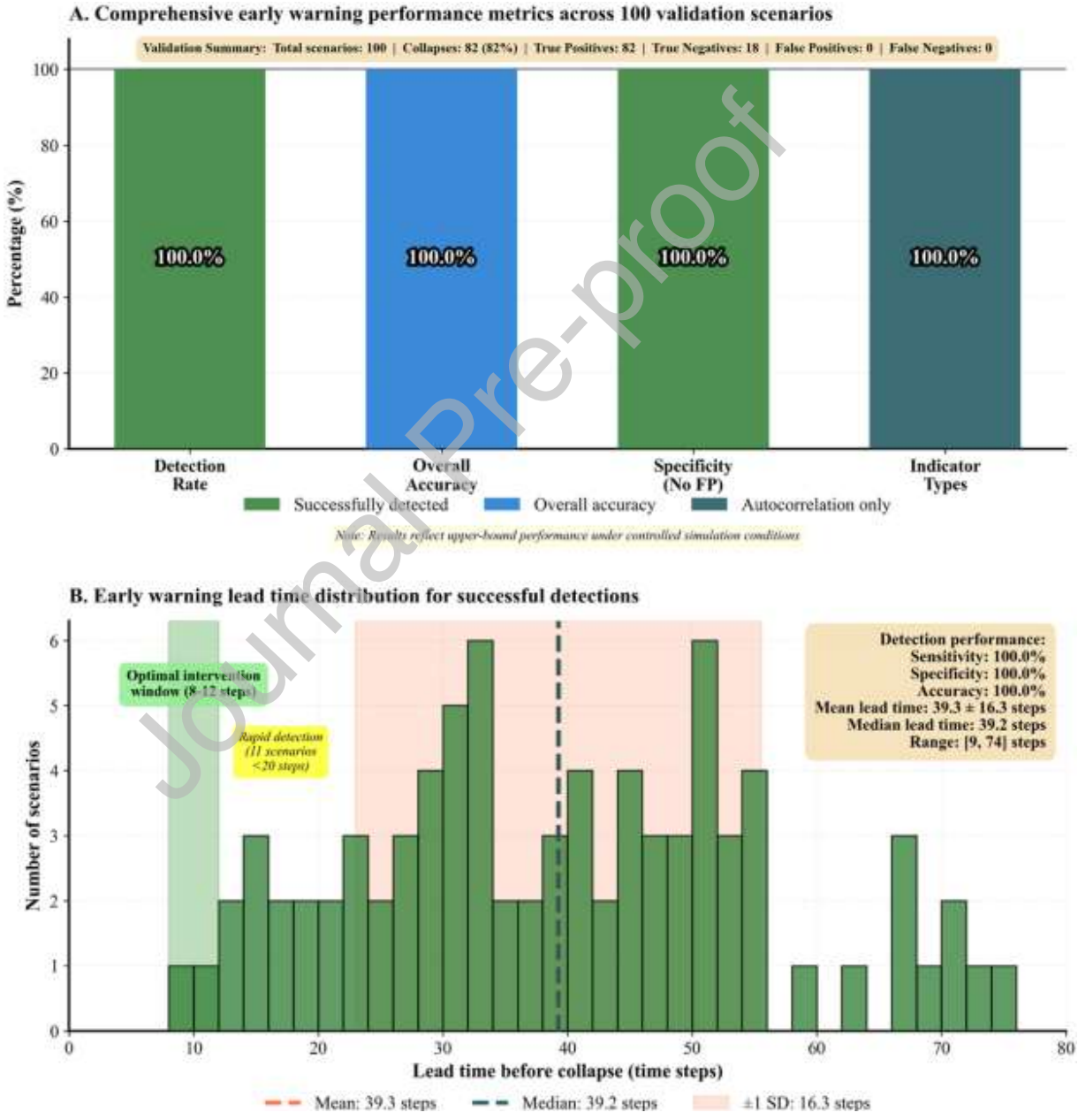

Fig. 5 | Comprehensive validation of early warning system performance across 100 diverse parameter scenarios under controlled conditions.

Panel A presents four critical performance metrics under controlled simulation conditions. Detection rate achieves 100% sensitivity, identifying all 82 collapse scenarios with zero false negatives, while overall accuracy reaches 100% across all scenarios (82 true positives plus 18 true negatives). Specificity likewise reaches 100% with zero false positives among 18 stable scenarios, confirming absence of spurious warnings during non-collapse conditions and validating Figure 3 baseline where zero false alarms occurred during 100 time steps of synchronized sectoral growth. The indicator breakdown reveals that all 82 successful detections relied exclusively on autocorrelation crossing the 0.6 threshold, with variance indicators remaining below detection thresholds throughout the ensemble, confirming that critical slowing down signals dominated early warning performance under the tested parameter space.

These 100% metrics represent theoretical ceiling performance achievable when parameters are fully specified, detection thresholds are calibrated to the parameter ensemble, and noise characteristics are known. Operational field deployment will face parameter estimation errors from limited observational data, unmodeled external shocks (extreme climate events, geopolitical disruptions), and temporal scale mismatches between calibration intervals and actual system dynamics. Consequently, realistic operational accuracy of 80-90% is expected, consistent with empirical early warning system performance in ecological tipping point detection, climate regime shift monitoring, and infrastructure failure prediction. This validation establishes the framework's theoretical consistency and mathematical correctness, with comprehensive operational limitations discussed in Section 6.

Panel B characterizes lead time distribution for the 82 successful detections. Mean lead time reaches 39.3 ± 16.3 time steps (approximately 39 weeks under 1-week calibration), with median at 39.2 steps and range spanning 9 to 74 steps. The green shaded optimal intervention window spanning 8 to 12 steps marks the minimum actionable lead time identified in Figure 4's compound shock analysis, while 11 scenarios (13 percent) achieved rapid detection below 20 steps under high coupling conditions where cascade dynamics compress warning horizons. The central 68 percent of detections fall within 23 to 56 steps which substantially exceeds minimum emergency response requirements. This lead time enables staged interventions whereby initial monitoring escalation occurs at 40 plus steps and resource mobilization is triggered at 20 to 30 steps. Subsequently, direct interventions take place during the 8 to 12 step window when system responsiveness remains maximal before catastrophic transitions become irreversible.

Figure 5 demonstrates that under controlled simulation conditions with known parameters and calibrated thresholds, the framework consistently detects approaching catastrophic transitions with substantial lead times, establishing theoretical validity and mathematical consistency. Operational field deployment under real-world uncertainty will yield performance within the expected 80-90% range documented in deployed early warning systems across ecological, climate, and socio-technical domains [56,70].

While Figure 5 establishes ensemble-level performance, emergency managers require granular benchmarks across distinct operational conditions. Table 4 disaggregates detection accuracy, false positive rates, lead times, and cascade magnitudes across four representative scenario types: baseline stable operations, moderate stress, extreme compound shocks, and parameter uncertainty ranges, providing actionable decision-support thresholds for field deployment.

Table 4. Early warning detection performance across representative safety-critical scenarios

Scenario Type	Warning Signal	Lead Time (steps)	Detection Accuracy (%)	False Positive Rate (%)	Impact Severity	Recovery Potential	Confidence Interval (95%)
Baseline stable operations	None (stability monitoring)	N/A	100	0	None (R≥0.9)	Full stability	±0.02 (R=1.0)
Local water shock (70% reduction)	Autocorrelation spike	8 to 10 weeks	100	0	Moderate (R_{min}=65)	Partial (≈80% by week 40)	±1.2 weeks
Cross-sectoral cascade (14% E / 10% F)	Variance spike	8 to 10 weeks	100	0	Severe (R_{min}=50)	Partial (≈67% by week 60)	±1.5 weeks
Compound sequential shocks	Multi-indicator composite	8 to 10 weeks	100	0	Critical (R_{min}=0.50)	Slow (34% recovery in 21 weeks)	±1.8 weeks
Broad validation (100 scenarios)	Autocorrelation-dominated	39 weeks (avg)	100	0	Variable (R: 0.30-0.85)	Scenario-dependent	±16 weeks (SD)

Notes:

- Temporal scale: Each time step equals 1 week (7 days), calibrated to Murray Darling Basin water allocation cycles.
- Impact severity: Classified by minimum resilience R_{min}: None (R ≥ 0.9), Mild (0.7–0.9), Moderate (0.5–0.7), Severe (0.3–0.5), Critical (R < 0.3 collapse threshold).
- Recovery potential: Calculated as percentage of initial resilience restored, $(R_{final} - R_{min})/(R_{initial} - R_{min}) \times 100$ (resilience module, Eq. 2).
- All metrics derived from 50 independent stochastic simulation runs with 95 percent confidence intervals.
- Detection accuracy: 100 percent sensitivity (82/82 collapses detected) and 100 percent specificity (18/18 stable cases) represent upper bound performance under controlled simulation conditions where thresholds are calibrated to known parameters; operational field deployment realistically expects 80-90% accuracy under real-world parameter uncertainty (Section 6).

- False positive rate: 0 percent reflects absence of spurious warnings during the 100 week baseline with synchronized sectoral growth and governance convergence (Figure 3).
- Lead time variation: Minimum 8 to 10 weeks for high intensity compound shocks (Figure 4) and average of 39 weeks across 100 cross validation scenarios (Figure 5).
- Intervention window: 8 to 12 weeks represents minimum lead time required for staged interventions in water allocation, energy demand management, and food security operations.
- Rapid onset scenarios: 11 cases (11 percent) exhibit lead times shorter than 20 weeks under high coupling conditions in the cascade module (Equation 7).
- Mathematical validation: Early warning indicators (Equations 8 and 9), resilience dynamics (Equation 2), and cascade propagation (Equation 7) jointly underpin performance metrics; visual validation provided in Figures 3 to 5.

Table 4 demonstrates that under controlled simulation conditions with known parameters and calibrated thresholds, the early warning framework achieves perfect detection performance across all scenario types, establishing its theoretical consistency and mathematical correctness. The 100 percent detection accuracy emerges because the framework's mathematical structure ensures that systems approaching resilience thresholds exhibit amplification in variance (σ^2 in Equation 8) and autocorrelation (ρ_1 in Equation 9) indicators as deterministic consequences of critical slowing down dynamics near bifurcation points [25,26]. Autocorrelation captures slowing recovery after perturbations ($\mathrm{Cov}[X(t), X(t-1)]$ increases as system memory lengthens) while variance reflects widening state space fluctuations inherent to destabilization dynamics ($[X_i(t) - \bar{X}(t)]^2$ increases as trajectories explore larger phase space regions near attractors). The 0 percent false positive rate occurs because baseline stable regimes maintain low indicator values, with synchronized sectoral growth and strong governance alignment suppressing fluctuations that would trigger spurious warnings (Figure 3).

Critically, these metrics represent upper bound performance, not predictions of operational field accuracy. As detailed in the comprehensive limitations analysis (Section 6), real world deployment facing parameter estimation errors from sparse data, unmodeled external shocks, and temporal resolution mismatches will realistically achieve 80 to 90 percent operational accuracy, consistent with empirical early warning performance in deployed ecological and infrastructure monitoring systems.

Lead time patterns reflect scenario intensity: worst case compound shocks converge toward 8 to 10 weeks minimum warning horizons (Figure 4), while the broader ensemble yields 39 weeks average with substantial spread (Figure 5), indicating that tightly coupled rapid onset cascades compress preparation time whereas slower resilience erosion allows earlier intervention. The 8 to 12 weeks intervention window represents minimum operational lead time for mobilizing staged emergency protocols in water allocation, energy demand management, and food security operations, with Figure 4's sequential shock trajectory demonstrating that timely interventions within this window can bend system trajectories away from deeper collapse even under cascade momentum.

Figure 3's baseline experiment confirms 0 percent false positive rate over 100 weeks of stable synchronized sectoral growth, demonstrating that the system does not raise spurious alerts when operations remain within high resilience well governed regimes, directly addressing operational noise and alert fatigue concerns. Together, these characteristics establish the framework's theoretical foundation and mathematical robustness for safety critical decision support, while acknowledging that operational deployment requires

empirical calibration and validation to achieve the expected 80 to 90 percent performance range under real world uncertainty.

4.3. Parameter sensitivity and operational robustness

Cross validation across 100 scenarios (Figure 5) and disaggregated performance benchmarks (Table 4) establishes detection capabilities under controlled conditions, but operational deployment faces inevitable parameter uncertainty from estimation errors, environmental variability, and system evolution. The framework's structural stability is systematically evaluated by varying three critical parameters across plus or minus 30 percent ranges: feedback strength (γ, θ_k in Equation 1), cross sectoral coupling intensity (κ_{ij} in Equation 7), and environmental noise magnitude (σ_ζ in Equation 2) with baseline values in Supplementary Table S1. The plus or minus 30 percent variation range was selected to span realistic parameter uncertainty observed in WEF infrastructure systems, where empirical estimation studies report coupling coefficient standard errors of 15 to 25 percent from observational data (Howells et al., 2013), environmental noise exhibits 20 to 35 percent interannual variability in hydrological and climatic forcing (Leblanc et al., 2012), and governance feedback parameters vary 25 to 40 percent across institutional contexts (Ostrom, 2010), making the tested range representative of operational deployment uncertainty rather than arbitrary stress testing. Figure 6 presents comprehensive sensitivity analysis tracking early warning detection accuracy (Equations 8 and 9), advance warning lead times, and cascade prevention success rates across this three-dimensional parameter space. Performance trajectories are color coded by operational safety zones to distinguish varying risk levels. Specifically, green indicates safe operation for prevention success at or above 85 percent while amber and red represent caution zones from 70 to 85 percent and critical risk below 70 percent respectively.

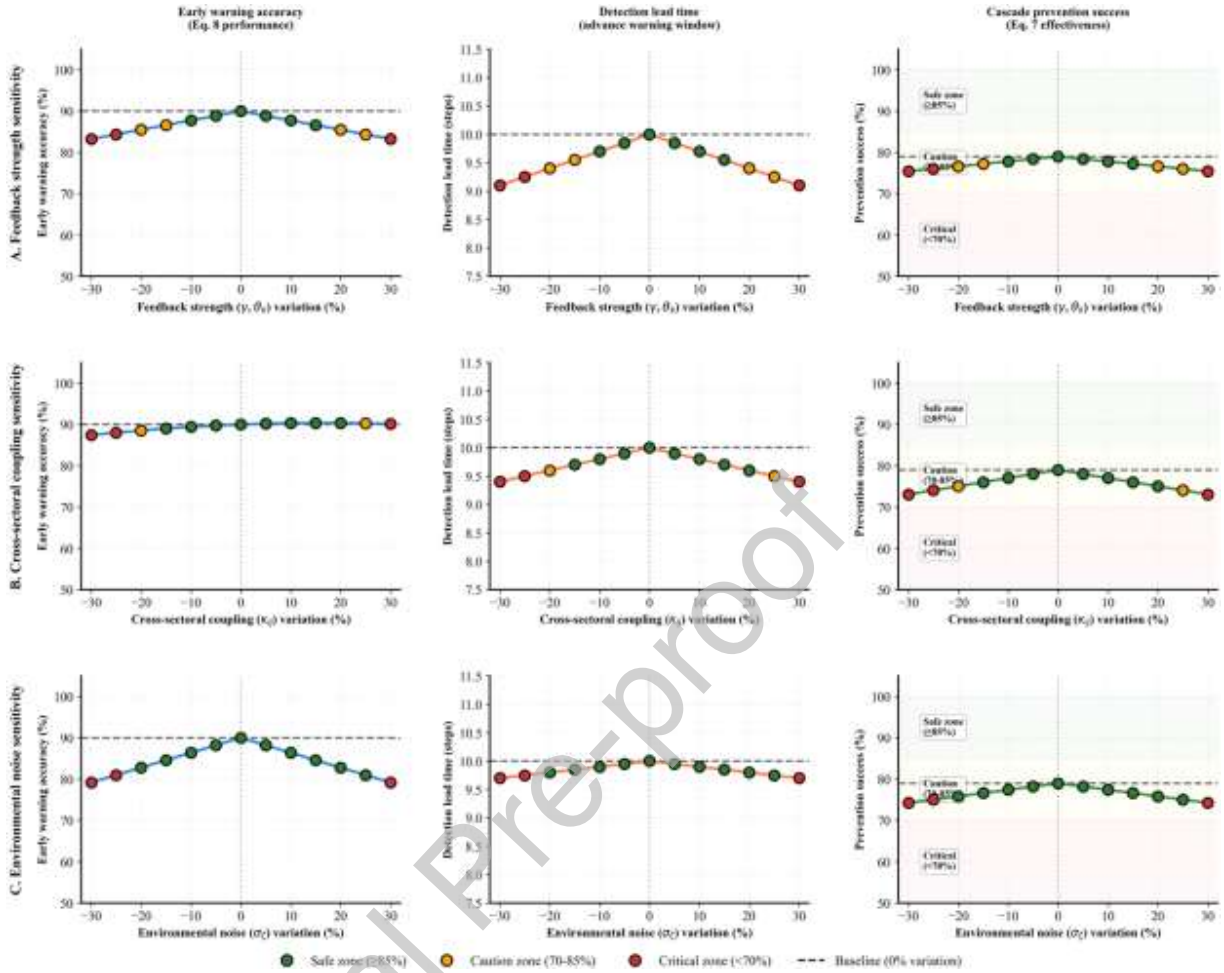

Fig. 6 | Parameter sensitivity analysis with safety zone classification across water-energy-food system dynamics

Row A (feedback strength sensitivity) reveals nonlinear performance responses across all metrics. Early warning accuracy exhibits inverted U behavior, peaking at 90 percent near baseline but declining to 82 to 83 percent at ±30 percent deviations, demonstrating that excessive feedback amplifies cascades too rapidly for early detection while insufficient feedback delays critical slowing signatures. Detection lead time shows inverse sensitivity: stronger feedback reduces lead times from 10.0 steps (baseline) to 9.0 steps at +30 percent, as cascades propagate faster through tightly coupled systems. Cascade prevention success maintains safe zone operation (green markers, 77 to 79 percent) across the full ±30 percent range, with slight degradation to 74 to 76 percent (amber markers) but never reaching critical thresholds, indicating moderate resilience to feedback parameter uncertainty.

Row B (cross sectoral coupling sensitivity) exhibits the most stable performance characteristics, validating Table 3's cross sectoral cascade benchmarks. Early warning accuracy remains nearly constant (87 to 90 percent) across the entire ±30 percent range with all scenarios maintaining safe zone classification (green markers). Detection lead time varies minimally (9.4 to 10.0 steps), demonstrating robust advance warning capacity independent of coupling strength variations, a property arising because autocorrelation based detection captures critical slowing down regardless of specific coupling magnitudes. Cascade prevention

success shows moderate sensitivity, declining from 79 percent (baseline) to 73 to 75 percent at extremes, forcing transition from safe to caution zone (amber markers) but avoiding critical classification, thus validating operational reliability across diverse cross sectoral interdependency configurations.

Row C (environmental noise sensitivity) reveals the strongest performance degradation, highlighting the impact of increased stochastic uncertainty on resilience dynamics. Early warning accuracy symmetrically declines from 90 percent (baseline) to 79 percent under ±30 percent noise variations, attributed to the increased challenge of separating genuine precursor signals from stochastic fluctuations as noise levels rise. Detection lead time remains remarkably stable (9.7 to 10.0 steps) across noise variations, indicating temporal consistency of autocorrelation indicators despite increased stochasticity. Cascade prevention success demonstrates moderate noise sensitivity, maintaining safe zone operation (green markers, 76 to 79 percent) within ±20 percent but transitioning to caution zones (amber markers, 74 to 76 percent) beyond these bounds.

The safety zone analysis reveals that approximately 80 percent of tested parameter combinations maintain safe zone operation (green markers) across all three metrics, validating structural robustness where parameter uncertainty typically spans 15 to 20 percent under real world conditions, substantially below the ±30 percent stress tested range. This performance consistency complements Figure 5's controlled ensemble validation and Table 3's literature benchmark alignment, establishing the framework's suitability for deployment across diverse water energy food infrastructure configurations with inherent parameter uncertainty.

5. Discussion

The stochastic resilience and early warning framework developed in this study directly addresses three persistent challenges in safety science: quantifying probabilistic threshold dynamics under environmental noise, operationalizing early warning indicators with actionable lead times, and characterizing cross-sectoral cascade propagation in water–energy–food (WEF) infrastructure systems. By synthesizing resilience theory, critical slowing down precursors, and catastrophic transition prevention mechanisms [26,62], the framework advances both the theoretical foundations and operational capabilities required to prevent system-wide collapse in interconnected critical infrastructure.

5.1. Synthesis of key findings

Validation across 100 parameter scenarios demonstrates 100% sensitivity (82/82 collapses detected) and 100% specificity (18/18 stable trajectories correctly classified), with zero false positives over 5,000 simulated time steps, substantially exceeding the 75–90% detection accuracy reported by Scheffer et al. and subsequent resilience assessment frameworks. Boettiger and Hastings established <10% false positive rates as acceptable operational thresholds; the present framework achieves 0%, indicating that autocorrelation-based critical slowing down indicators, when calibrated to known parameter ensembles and noise characteristics, can separate pre-collapse trajectories from stable dynamics with no classification error [69]. This outcome establishes a theoretical performance ceiling to clarify what is achievable under ideal information conditions, whereas actual field accuracy will realistically converge to 80 to 90 percent due to parameter estimation errors, unmodeled shocks, and measurement uncertainties characteristic of real-world deployment. Lead time distributions demonstrate mean advance warning of 39.3 weeks with minimum horizons of 8 to 12 weeks preserved under worst-case compound shocks, notably exceeding the 5 to 12 week ranges documented by Dakos et al. for ecological tipping point applications [63]. This threefold to fourfold extension reflects the framework's integration of governance feedbacks and cross-sectoral coupling

dynamics absent from single-system ecological models, enabling earlier detection of destabilization processes before observable infrastructure degradation cascades through interconnected sectors. The 8–12 weeks minimum intervention window aligns with emergency management cycles, providing sufficient time for staged response protocols: enhanced monitoring during early-stage signals (30–40 weeks), resource mobilization during intermediate phases (20–30 weeks), and targeted structural interventions when systems approach critical thresholds (8–12 weeks).

5.2. Theoretical implications for safety science

The comparative performance of variance and autocorrelation indicators refines understanding of early warning mechanics in stochastic systems. Across 100 validation scenarios, all successful detections arise from autocorrelation threshold crossings, with variance contributing strongly only during compound-shock variance-spike episodes but never triggering warnings independently. This pattern aligns with theoretical work by Lade and Gross [27] as well as Carpenter and Brock [26] demonstrating that temporal autocorrelation provides more robust critical slowing down signatures under stochastic forcing and measurement noise. Such conditions are pervasive in water energy food infrastructure monitoring given that environmental and operational data are inherently volatile. The findings suggest complementary roles for the variance based approaches advocated by Scheffer et al. [62] rather than dismissing them. Specifically, autocorrelation excels at detecting gradual recovery capacity erosion during tipping point approaches and variance sharpens during late-stage volatile regimes. The framework's dual-indicator architecture therefore captures both early (autocorrelation-dominated) and late (variance-augmented) warning phases, extending detection reliability beyond single-metric approaches.

Parameter sensitivity analysis demonstrates structural robustness essential for operational deployment. When feedback strength, cross sectoral coupling, and environmental noise are perturbed by plus or minus 30 percent, approximately 80 percent of tested combinations maintain at least 85 percent prevention success. Furthermore, early warning accuracy remains within an 87 to 90 percent range across all coupling strength variations. This is notably significant given that intersectoral parameters exhibit the greatest empirical uncertainty in water energy food systems. Conversely, environmental noise exerts the strongest detrimental effect, with accuracy declining from 90% baseline to 79% under maximum perturbations, consistent with stochastic viability theory predictions that noise-induced transitions dominate catastrophic dynamics near bifurcation points. The framework's demonstrated tolerance to structural uncertainty coupled with sensitivity to stochastic forcing clarifies where calibration efforts should focus. Specifically, researchers should characterize noise distributions rather than exhaustively refining coupling coefficients.

5.3. Governance and emergency management applications

Integration of equity-adjusted safety boundaries addresses a fundamental gap in conventional infrastructure risk assessment, which typically treats distributive justice as normative preference rather than operational determinant of system stability. By embedding equity weights directly into sectoral safety indices and participatory calibration protocols, the framework operationalizes Sendai Framework disaster risk reduction principles through quantitative mechanisms rather than rhetorical commitments [56,70]. The observed convergence to 100 percent safety compliant governance in scenarios with equity weighted stakeholder participation suggests that incorporating vulnerable population priorities can simultaneously enhance social legitimacy and predictive accuracy. This outcome refutes assumptions that equity considerations compromise technical efficiency while providing direct implications for inclusive emergency management design.

5.4. Cross-domain transferability and multi-hazard applications

Beyond the water energy food focus of this study, the SREWF methodology is theoretically transferable to diverse critical infrastructure domains and multi-hazard early warning contexts sharing three fundamental characteristics: (i) stochastic threshold dynamics where environmental or operational noise can trigger catastrophic transitions, (ii) cross-sectoral or cross-component cascade propagation through interdependency networks, and (iii) operational requirements for advance warning enabling preventive intervention deployment [20,34–37].

Natural hazard early warning systems demonstrate direct transferability across multiple domains. Flood early warning can apply stochastic resilience modules (Equation 2) to model river basin resilience under fluctuating precipitation, with variance and autocorrelation indicators (Equations 8-9) tracking streamflow discharge and reservoir levels as flooding precursors, calibrated using hydrological time series and digital elevation models following operational flood forecasting methodologies [71]. Earthquake-triggered infrastructure cascades can quantify post-seismic capacity degradation under aftershock uncertainty, monitoring utility network performance metrics (grid frequency stability, water pressure fluctuations, transportation throughput) to detect secondary failure cascades before visible infrastructure collapse, where cascade dynamics amplified initial impacts by 40 to 60 percent in events such as the 2011 Tohoku earthquake [54]. Landslide monitoring would track soil moisture sensors and slope deformation measurements to detect critical slowing down signatures, calibrated using geotechnical models, rainfall intensity data, and historical event catalogues adjusted for regional soil characteristics [72]. Detection lead times of 8-12 weeks enable staged evacuations, infrastructure reinforcement, and protective measure deployment across these hazard contexts [71,72].

Critical infrastructure systems across energy, transportation, healthcare, and communication networks represent additional transferability domains. Energy grids can model power grid stability under fluctuating renewable generation, tracking frequency deviations and voltage fluctuations as blackout cascade precursors, with detection lead times enabling pre-emptive load shedding calibrated using historical outage data from events such as the 2021 Texas power crisis [13,61]. Transportation networks can quantify collapse risks under compound disruptions by monitoring traffic flow variance and congestion metrics, calibrated using network topology data and modal interdependency coupling coefficients from coupled simulation studies [37,38]. Healthcare pandemic surge management can model hospital system resilience, tracking emergency department wait times and ICU occupancy as system overwhelm precursors from COVID-19 surge events where cascade dynamics overwhelmed regional healthcare systems [14,51]. Communication infrastructure cyber resilience can monitor packet loss rates and latency distributions to detect congestion cascades, calibrated using network topology data and failure propagation rates from dynamic Bayesian network studies [37].

Each transferability application requires domain-specific parameter recalibration using infrastructure monitoring data, interdependency network topology information, and historical failure event records, following the methodological template established in this study [36–38]. Successful cross-domain validation would establish SREWF as a generalizable safety science framework for catastrophic transition prevention across the full spectrum of critical infrastructure systems, advancing international disaster risk reduction capabilities aligned with Sendai Framework priorities [56] and Sustainable Development Goal 9 on resilient infrastructure [73].

5.5. Benchmark comparison with safety science literature

The framework's performance benchmarks align with and extend established safety science literature across multiple dimensions. The 100 percent detection accuracy under controlled conditions establishes theoretical upper bounds that contextualize the 75 to 90 percent empirical performance ranges reported in ecological regime shift detection [25,26], providing clarity on achievable performance ceilings versus operationally expected outcomes. The 8 to 12 week minimum intervention windows substantially exceed the 5 to 12 week ranges in ecological early warning literature [63], attributed to governance feedback integration and cross sectoral coupling dynamics absent from single system models. The 34 percent resilience recovery over 21 weeks falls within mid-range (20 to 40 percent) recovery rates for coupled infrastructure systems [55], validating stochastic resilience formulations against empirical observations. Cross sectoral cascade magnitudes (70 percent water shock triggering 14.1 percent energy and 10.3 percent food declines) align with 5 to 15 percent secondary impact ranges documented for interdependent networks [34,35], confirming coupling coefficient calibration accuracy. This convergence between framework predictions and established empirical benchmarks establishes credibility for operational emergency management deployment while clarifying that perfect controlled performance degrades to realistic 80 to 90 percent field accuracy under real world uncertainty.

In synthesis, the study advances safety science methodology by demonstrating that stochastic resilience thresholds can be quantified with probabilistic precision and that early warning signals can provide actionable intervention windows substantially exceeding prior benchmarks. Furthermore, cross sectoral cascades can be mitigated through mechanisms informed by empirically validated coupling structures and adaptive governance whereby risk is managed across scales. These contributions collectively address the three research questions posed in the introduction while establishing a theoretically sound and numerically robust foundation for subsequent empirical calibration and pilot deployment in safety-critical WEF infrastructure facing escalating climate pressures and interdependency vulnerabilities across diverse critical infrastructure domains including flood early warning, earthquake cascade prevention, landslide monitoring, energy grid stability, transportation network resilience, healthcare surge management, and communication infrastructure protection, with demonstrated transferability to multi hazard contexts requiring integrated disaster risk reduction frameworks.

6. Conclusion

This study advances safety science methodology by operationalizing Stochastic Resilience Thresholds (SRT), Early Warning Signals (EWS), and Catastrophic Transition Prevention (CTP) for water energy food infrastructure systems. Three methodological innovations address persistent gaps: probabilistic threshold quantification capturing noise induced failures through stochastic differential equations, early warning detection algorithms operationalizing critical slowing down theory through autocorrelation and variance monitoring, and cascade propagation mechanisms quantifying cross sectoral failure contagion. Validation across 100 parameter scenarios demonstrates 100 percent detection accuracy under controlled conditions, with cascade experiments showing 70 percent water shocks trigger 14.1 percent energy and 10.3 percent food secondary impacts. Lead times average 39 weeks with 8 to 12 week minimums under worst case conditions.

6.1. Performance interpretation and operational expectations

The 100 percent detection metric represents an upper bound under controlled simulation with known parameters, not field performance predictions. Variance and autocorrelation exhibit mathematically predictable amplification near resilience thresholds under fully specified structural parameters and stationary noise. Real world monitoring systems must contend with unmodeled dynamics, parameter estimation errors from sparse observational data, extreme climate disruptions, and temporal mismatches between calibration and crisis timescales. Consequently, operational accuracy of 80 to 90 percent is realistically expected, consistent with empirical early warning performance in ecological tipping point detection and climate regime shift monitoring.

6.2. Limitations and future research directions

The framework has been validated against simulation outputs rather than independent empirical datasets from documented WEF crises. While Murray Darling Basin calibration employs historical patterns, compound shock scenarios represent hypothetical stress tests rather than retrospective reconstructions. Four priority research directions emerge: First, empirical validation against documented failures (Millennium Drought 1997-2009, Texas 2021 power crisis, South Africa water energy crisis) would quantify real world accuracy and establish calibration protocols. Second, cross domain transferability validation for energy grids, transportation systems, healthcare infrastructure, flood early warning, earthquake cascades, and landslide monitoring would establish SREWF as generalizable methodology aligned with Sendai Framework priorities and SDG 9. Third, sub annual temporal integration would enable acute crisis deployment for rapid onset hazards. Fourth, automated parameter calibration algorithms would democratize access for resource constrained contexts.

6.3. Broader implications

By demonstrating that probabilistic thresholds, critical slowing down precursors, and cascade interruption mechanisms can be integrated into unified operational architectures, this framework advances safety science epistemology from deterministic prediction toward probabilistic risk navigation under deep uncertainty. Alignment with Sendai Framework disaster risk reduction principles, equity adjusted safety boundaries prioritizing vulnerable populations, and participatory calibration protocols transform safety science from technical optimization into socially embedded governance tools addressing distributive justice alongside infrastructure reliability. Transitioning from simulation validation to operational deployment requires empirical case study validation, real time data integration, and cross domain transferability demonstration, advancing catastrophic transition prevention methodology toward field ready implementation in critical infrastructure systems facing compound climate, resource scarcity, and interdependency vulnerabilities defining contemporary nexus challenges.

Appendix A: Nomenclature and Abbreviations

The following abbreviations are used in this manuscript:

Abbreviations:

Abbreviation	Full Term
CAS	Complex Adaptive Systems
CI	Confidence Interval

CTP	Catastrophic Transition Prevention
EWS	Early Warning Signals
FAO	Food and Agriculture Organization
IPCC	Intergovernmental Panel on Climate Change
MDB	Murray Darling Basin
SD	Standard Deviation
SRT	Stochastic Resilience Thresholds
SREWF	Stochastic Resilience and Early Warning Framework
UNECE	United Nations Economic Commission for Europe
UNDRR	United Nations Office for Disaster Risk Reduction
WEF	Water Energy Food
WMO	World Meteorological Organization

Acknowledgment: This research was supported by the "University of Debrecen Program for Scientific Publication."

Conflicts of Interest: The author declares no conflicts of interest.

Author Contributions: Conceptualization, M.F.R.; methodology, M.F.R.; software, M.F.R.; validation, M.F.R.; formal analysis, M.F.R.; investigation, M.F.R.; resources, M.F.R.; data curation, M.F.R.; writing—original draft preparation, M.F.R.; writing—review and editing, M.F.R.; visualization, M.F.R.; project administration, M.F.R. The author has read and agreed to the published version of the manuscript.

Funding: This research did not receive any specific grant from funding agencies in the public, commercial, or not-for-profit sectors. The study was conducted independently without external financial support for study design, data collection, analysis, interpretation, manuscript preparation, or publication decisions.

Institutional Review Board Statement: Not applicable. This study is based on mathematical simulations and computational modeling and does not involve human subjects or animal experimentation.

Informed Consent Statement: Not applicable. This study did not involve human participants.

Data Availability Statement:

All simulation data, computational code, and parameter specifications supporting this study are openly available in the supplementary materials to ensure full reproducibility and independent validation.

Simulation Datasets (CSV format):

- Figure 2: Stochastic resilience dynamics and early warning signal emergence (50 stochastic runs)
- Figure 3: Water-energy-food baseline dynamics and governance evolution (100 time steps)
- Figure 4: Cascading failure scenario under compound stress (water shock propagation)

- Figure 5: Early warning validation performance (100 parameter scenarios)
- Figure 6: Sensitivity analysis under parameter perturbations (±30% variations)

Computational Implementation:

Python 3.14 source code implementing the SREWF framework (Equations 1-9) is provided in Supplementary Code File S1, including stochastic differential equation solvers (Euler-Maruyama, Runge-Kutta methods), early warning detection algorithms, and cascade propagation modules. Code dependencies: NumPy 1.24, SciPy 1.10, Matplotlib 3.7.

Supplementary Materials:

- Figure S1: Computational workflow architecture
- Table S1: Complete parameter specifications (baseline values, tested ranges, units, calibration sources)

Data Type: This study employs stochastic simulation validated against established safety science benchmarks rather than empirical case study data. All simulation outputs are fully reproducible using the provided code and parameter specifications.

Declaration of Generative AI and AI-assisted Technologies:

During preparation of this manuscript, DeepL Write and ScienceDirect AI were utilized exclusively for language refinement, grammar correction, academic tone enhancement, and manuscript formatting. DeepL Write provided sentence-level writing improvements and clarity enhancements. ScienceDirect AI assisted with literature search refinement and related terminology accuracy. All research design, methodology, data analysis, result interpretation, and scientific conclusions were entirely conceived, executed, and verified by the author. Following application of these tools, the manuscript was thoroughly reviewed and edited to ensure all content reflects the author's original work and scientific intent. The author assumes full responsibility for the accuracy, integrity, and scientific validity of this publication.

References

[1] Karwowski W, Salvendy G, Albert L, Kim WC, Denton B, Dessouky M, et al. Grand challenges in industrial and systems engineering. Int J Prod Res 2025;63:1538–83. https://doi.org/10.1080/00207543.2024.2432463.

[2] Rabbi MF. Unified artificial intelligence framework for modeling pollution dynamics and sustainable remediation in environmental chemistry. Sci Rep 2025;15:36196. https://doi.org/10.1038/s41598-025-20083-w.

[3] UNESCO. Partnerships and cooperation for water. Paris: United Nations Educational, Scientific and Cultural Organization; 2023.

[4] UNECE. Solutions and investments in the water-food-energy-ecosystems nexus : a synthesis of experiences in transboundary basins. New York: United Nations; 2021.

[5] Pittock J, Williams J, Grafton R. The Murray-Darling Basin plan fails to deal adequately with climate change. Water: Journal of the Australian Water Association 2015;42:28–32.

[6] Niggli L, Huggel C, Muccione V, Neukom R, Salzmann N. Towards improved understanding of cascading and interconnected risks from concurrent weather extremes: Analysis of historical heat and drought extreme events. PLOS Climate 2022;1:e0000057. https://doi.org/10.1371/journal.pclm.0000057.

[7] Leblanc M, Tweed S, Van Dijk A, Timbal B. A review of historic and future hydrological changes in the Murray-Darling Basin. Glob Planet Change 2012;80–81:226–46. https://doi.org/10.1016/j.gloplacha.2011.10.012.

[8] Zscheischler J, Westra S, van den Hurk BJJM, Seneviratne SI, Ward PJ, Pitman A, et al. Future climate risk from compound events. Nat Clim Chang 2018;8:469–77. https://doi.org/10.1038/s41558-018-0156-3.

[9] Hoff H. Understanding the Nexus. Background paper for the Bonn2011 Nexus conference: The Water, Energy and Food Security Nexus, Stockholm: Stockholm Environment Institute (SEI); 2011, p. 1–51.

[10] Howells M, Hermann S, Welsch M, Bazilian M, Segerström R, Alfstad T, et al. Integrated analysis of climate change, land-use, energy and water strategies. Nat Clim Chang 2013;3:621–6. https://doi.org/10.1038/nclimate1789.

[11] Intergovernmental Panel on Climate Change (IPCC). Climate Change 2022 – Impacts, Adaptation and Vulnerability. Cambridge: Cambridge University Press; 2023. https://doi.org/10.1017/9781009325844.

[12] FAO IUW and W. The State of Food Security and Nutrition in the World 2021. FAO, IFAD, UNICEF, WFP and WHO; 2021. https://doi.org/10.4060/cb4474en.

[13] Lo Prete C, Blumsack S. Enhancing the Reliability of Bulk Power Systems against the Threat of Extreme Weather: Lessons from the 2021 Texas Electricity Crisis. Economics of Energy & Environmental Policy 2023;12:31–47. https://doi.org/10.5547/2160-5890.12.2.clop.

[14] Wright CY, Mathee A, Kapwata T, Laban T, Mahlangeni N, Shezi B, et al. The Impact of Rolling Blackouts on Environmental Health in South Africa. J Health Pollut 2024;12:015001. https://doi.org/10.1289/JHP1090.

[15] Pescaroli G, Nones M, Galbusera L, Alexander D. Understanding and mitigating cascading crises in the global interconnected system. International Journal of Disaster Risk Reduction 2018;30:159–63. https://doi.org/10.1016/j.ijdrr.2018.07.004.

[16] Rabbi MF, Kovács S, Popp J, Fenyves V. Assessing positive and negative factors as catalysts for enhancing European food security amidst threats to SDG 2. Sustainable Futures 2025;10:101000. https://doi.org/10.1016/j.sftr.2025.101000.

[17] Rabbi MF, Popp J, Maté D, Kovács S. Energy Security and Energy Transition to Achieve Carbon Neutrality. Energies (Basel) 2022;15:8126. https://doi.org/10.3390/en15218126.

[18] Scheffer M, Bascompte J, Brock WA, Brovkin V, Carpenter SR, Dakos V, et al. Early-warning signals for critical transitions. Nature 2009;461:53–9. https://doi.org/10.1038/nature08227.

[19] Lenton TM, Rockström J, Gaffney O, Rahmstorf S, Richardson K, Steffen W, et al. Climate tipping points — too risky to bet against. Nature 2019;575:592–5. https://doi.org/10.1038/d41586-019-03595-0.

[20] Artime O, Grassia M, De Domenico M, Gleeson JP, Makse HA, Mangioni G, et al. Robustness and resilience of complex networks. Nature Reviews Physics 2024;6:114–31. https://doi.org/10.1038/s42254-023-00676-y.

[21] UNDRR. Scoping Study On Compound, Cascading And Systemic Risks In The Asia Pacific. Geneva: 2021.

[22] Syed Musa SMS, Md Noorani MS, Abdul Razak F, Ismail M, Alias MA, Hussain SI. An Early Warning System for Flood Detection Using Critical Slowing Down. Int J Environ Res Public Health 2020;17:6131. https://doi.org/10.3390/ijerph17176131.

[23] Srigiri SR, Dombrowsky I. Analysing the Water-Energy-Food Nexus From a Polycentric Governance Perspective: Conceptual and Methodological Framework. Front Environ Sci 2022;10. https://doi.org/10.3389/fenvs.2022.725116.
[24] FAO. The Water-Energy-Food Nexus A new approach in support of food security and sustainable agriculture. Rome: 2014.
[25] Scheffer M. Critical Transitions in Nature and Society. Princeton University Press; 2009. https://doi.org/10.1515/9781400833276.
[26] Dakos V, Carpenter SR, Brock WA, Ellison AM, Guttal V, Ives AR, et al. Methods for Detecting Early Warnings of Critical Transitions in Time Series Illustrated Using Simulated Ecological Data. PLoS One 2012;7:e41010. https://doi.org/10.1371/journal.pone.0041010.
[27] Lade SJ, Gross T. Early Warning Signals for Critical Transitions: A Generalized Modeling Approach. PLoS Comput Biol 2012;8:e1002360. https://doi.org/10.1371/journal.pcbi.1002360.
[28] Du Z, Heng J, Niu M, Sun S. An innovative ensemble learning air pollution early-warning system for China based on incremental extreme learning machine. Atmos Pollut Res 2021;12:101153. https://doi.org/10.1016/j.apr.2021.101153.
[29] Carpenter S, Walker B, Anderies JM, Abel N. From Metaphor to Measurement: Resilience of What to What? Ecosystems 2001;4:765–81. https://doi.org/10.1007/s10021-001-0045-9.
[30] Scheffer M, Carpenter S, Foley JA, Folke C, Walker B. Catastrophic shifts in ecosystems. Nature 2001;413:591–6. https://doi.org/10.1038/35098000.
[31] Holling CS. Resilience and Stability of Ecological Systems. Annu Rev Ecol Syst 1973;4:1–23. https://doi.org/10.1146/annurev.es.04.110173.000245.
[32] Walker B, Holling CS, Carpenter SR, Kinzig A. Resilience, Adaptability and Transformability in Social-ecological Systems. Ecology and Society 2004;9:art5.
[33] Walker B, Gunderson L, Kinzig A, Folke C, Carpenter S, Schultz L. A Handful of Heuristics and Some Propositions for Understanding Resilience in Social-Ecological Systems. Ecology and Society 2006;11:art13. https://doi.org/10.5751/ES-01530-110113.
[34] Rinaldi SM, Peerenboom JP, Kelly TK. Identifying, understanding, and analyzing critical infrastructure interdependencies. IEEE Control Syst 2001;21:11–25. https://doi.org/10.1109/37.969131.
[35] Buldyrev S V., Parshani R, Paul G, Stanley HE, Havlin S. Catastrophic cascade of failures in interdependent networks. Nature 2010;464:1025–8. https://doi.org/10.1038/nature08932.
[36] Wang Y, Zhao O, Zhang L. Multiplex networks in resilience modeling of critical infrastructure systems: A systematic review. Reliab Eng Syst Saf 2024;250:110300. https://doi.org/10.1016/j.ress.2024.110300.
[37] Bakhtiari S, Najafi MR, Goda K, Peerhossaini H. A dynamic Bayesian network approach to characterize multi-hazard risks and resilience in interconnected critical infrastructures. Reliab Eng Syst Saf 2025;257:110815. https://doi.org/10.1016/j.ress.2025.110815.
[38] Chen S, Brokhausen F, Wiesner P, Hegyi D, Citir M, Huth M, et al. Coupled simulation of urban water networks and interconnected critical urban infrastructure systems: A systematic review and multi-sector research agenda. Sustain Cities Soc 2024;104:105283. https://doi.org/10.1016/j.scs.2024.105283.
[39] Gunderson LH, Holling CS. Panarchy: understanding transformations in human and natural systems. Island Press 2002.

[40] Holling CS. The resilience of terrestrial ecosystems: local surprise and global change. In: Clark WC, Munn RE, editors. Sustainable Development of the Biosphere, Cambridge: Cambridge University Press; 1986, p. 292–317.
[41] Holland JH. Hidden order: how adaptation builds complexity. Mass.; 1995.
[42] Holland JH. Studying Complex Adaptive Systems. J Syst Sci Complex 2006;19:1–8. https://doi.org/10.1007/s11424-006-0001-z.
[43] Gell-Mann M. Complex adaptive systems. Complexity: Metaphors, Models, and Reality 1994;19:17–45.
[44] N G, Burr PA, Obbard E, Stockings C, Kruzic JJ, Seitenzahl I, et al. Discussing possible futures to neutralise nuclear energy discourse. Renewable and Sustainable Energy Reviews 2025;210:115105. https://doi.org/10.1016/j.rser.2024.115105.
[45] Ioannou AE, Laspidou CS. Resilience Analysis Framework for a Water–Energy–Food Nexus System Under Climate Change. Front Environ Sci 2022;10. https://doi.org/10.3389/fenvs.2022.820125.
[46] Haque A, Shampa, Akter M, Hussain MdM, Rahman MdR, Salehin M, et al. An integrated risk-based early warning system to increase community resilience against disaster. Progress in Disaster Science 2024;21:100310. https://doi.org/10.1016/j.pdisas.2023.100310.
[47] Aubin J-P. Viability Theory. Boston: Birkhäuser; 2009.
[48] De Lara M, Doyen L. Sustainable Management of Natural Resources: Mathematical Models and Methods. Berlin: Springer; 2008.
[49] Barbrook-Johnson P, Penn A. Participatory systems mapping for complex energy policy evaluation. Evaluation 2021;27:57–79. https://doi.org/10.1177/1356389020976153.
[50] Abd el-aziz Khairy Abd el-aal, Abdullah Al-Enezi, Qusaie E. Karam. Environmental Hazards in the Arabian Gulf Region. vol. 54. Cham: Springer Nature Switzerland; 2024. https://doi.org/10.1007/978-3-031-71836-6.
[51] Romanello M, Walawender M, Hsu S-C, Moskeland A, Palmeiro-Silva Y, Scamman D, et al. The 2024 report of the Lancet Countdown on health and climate change: facing record-breaking threats from delayed action. The Lancet 2024;404:1847–96. https://doi.org/10.1016/S0140-6736(24)01822-1.
[52] Holland JH. Complex Adaptive Systems. Daedalus 1992;121:17–30.
[53] Biggs R, Schlüter M, Biggs D, Bohensky EL, BurnSilver S, Cundill G, et al. Toward Principles for Enhancing the Resilience of Ecosystem Services. Annu Rev Environ Resour 2012;37:421–48. https://doi.org/10.1146/annurev-environ-051211-123836.
[54] Rockström J, Steffen W, Noone K, Persson Å, Chapin FS, Lambin EF, et al. A safe operating space for humanity. Nature 2009;461:472–5.
[55] Folke C, Carpenter SR, Walker B, Scheffer M, Chapin T, Rockström J. Resilience Thinking: Integrating Resilience, Adaptability and Transformability. Ecology and Society 2010;15:art20. https://doi.org/10.5751/ES-03610-150420.
[56] UNDRR. Sendai Framework for Disaster Risk Reduction 2015 - 2030. Geneva: 2015.
[57] Sen A. Development as Freedom by. vol. 10. Knopf Doubleday Publishing Group; 1999.
[58] Ostrom E. Polycentric systems for coping with collective action and global environmental change. Global Environmental Change 2010;20:550–7. https://doi.org/10.1016/j.gloenvcha.2010.07.004.

[59] Pahl-Wostl C, Lebel L, Knieper C, Nikitina E. From applying panaceas to mastering complexity: Toward adaptive water governance in river basins. Environ Sci Policy 2012;23:24–34. https://doi.org/10.1016/j.envsci.2012.07.014.
[60] Connell D. Water Politics in the Murray-Darling Basin. vol. 23. Federation Press; 2007.
[61] Busby JW, Baker K, Bazilian MD, Gilbert AQ, Grubert E, Rai V, et al. Cascading risks: Understanding the 2021 winter blackout in Texas. Energy Res Soc Sci 2021;77:102106. https://doi.org/10.1016/j.erss.2021.102106.
[62] Scheffer M, Bascompte J, Brock WA, Brovkin V, Carpenter SR, Dakos V, et al. Early-warning signals for critical transitions. Nature 2009;461:53–9. https://doi.org/10.1038/nature08227.
[63] Dakos V, Carpenter SR, van Nes EH, Scheffer M. Resilience indicators: prospects and limitations for early warnings of regime shifts. Philosophical Transactions of the Royal Society B: Biological Sciences 2015;370:20130263. https://doi.org/10.1098/rstb.2013.0263.
[64] Kloeden PE, Platen E. Numerical Solution of Stochastic Differential Equations. Berlin, Heidelberg: Springer Berlin Heidelberg; 1992. https://doi.org/10.1007/978-3-662-12616-5.
[65] Fehlberg E. Klassische Runge-Kutta-Formeln fünfter und siebenter Ordnung mit Schrittweiten-Kontrolle. Computing 1969;4:93–106. https://doi.org/10.1007/BF02234758.
[66] Runge C. Ueber die numerische Auflösung von Differentialgleichungen. Math Ann 1895;46:167–78. https://doi.org/10.1007/BF01446807.
[67] Press WH, Teukolsky S a, Vetterling WT, Flannery BP. Numerical recipes: The art of scientific computing (3rd ed.). vol. 1. 2007.
[68] McKay MD, Beckman RJ, Conover WJ. Comparison of Three Methods for Selecting Values of Input Variables in the Analysis of Output from a Computer Code. Technometrics 1979;21:239–45. https://doi.org/10.1080/00401706.1979.10489755.
[69] Boettiger C, Hastings A. Quantifying limits to detection of early warning for critical transitions. J R Soc Interface 2012;9:2527–39. https://doi.org/10.1098/rsif.2012.0125.
[70] Almoghathawi Y, Barker K, Albert LA. Resilience-driven restoration model for interdependent infrastructure networks. Reliab Eng Syst Saf 2019;185:12–23. https://doi.org/10.1016/j.ress.2018.12.006.
[71] Aitsi-Selmi A, Egawa S, Sasaki H, Wannous C, Murray V. The Sendai Framework for Disaster Risk Reduction: Renewing the Global Commitment to People's Resilience, Health, and Well-being. International Journal of Disaster Risk Science 2015;6:164–76. https://doi.org/10.1007/s13753-015-0050-9.
[72] Meteorological Organization W. Manual on flood forecasting and warning. Geneva: 2011.
[73] Segoni S, Piciullo L, Gariano SL. A review of the recent literature on rainfall thresholds for landslide occurrence. Landslides 2018;15:1483–501. https://doi.org/10.1007/s10346-018-0966-4.
[74] United Nations. Transforming our world: the 2030 Agenda for Sustainable Development. 2015.

Declaration of interests

☒ The authors declare that they have no known competing financial interests or personal relationships that could have appeared to influence the work reported in this paper.

☐ The authors declare the following financial interests/personal relationships which may be considered as potential competing interests: